Fragility functions for masonry infill walls with in-plane loading

Andrea Chiozzi [a]*, Eduardo Miranda [b]

[a] *Department of Engineering, University of Ferrara,*
1 Via Saragat, Ferrara, 44122, Italy
E-mail: *andrea.chiozzi@unife.it*
(*) Corresponding author.

[b] *Department of Civil and Environmental Engineering, Stanford University*
473 Via Ortega, Stanford, CA 94305-4020, USA
E-mail: *emiranda@stanford.edu*

Keywords: Fragility functions; Masonry infill walls; Damage estimation; Seismic performance assessment

ABSTRACT

Recent seismic events have provided evidence that damage to masonry infills can lead not only to large economic losses but also to significant injuries and even fatalities. The estimation of damage of such elements and the corresponding consequences within the Performance-Based Earthquake Engineering framework, requires the construction of reliable fragility functions. In this paper, drift-based fragility functions are developed for in-plane loaded masonry infills, derived from a comprehensive experimental dataset gathered from current literature, comprising 152 masonry infills with different geometries and built with different types of masonry blocks, when tested under lateral cyclic loading. Three damage states associated with the structural performance and reparability of masonry infill walls are defined. The effect of mortar compression strength, masonry prism compression strength and presence of openings is evaluated and incorporated for damage states where their influence is found to be statistically significant. Uncertainty due to specimen-to-specimen variability and sample size is quantified and included in the proposed fragility functions. It is concluded that prism strength and mortar strength are better indicators of the fragility of masonry infills than the type of bricks/blocks employed, whose influence, in general, is not statistically significant for all damage states. Finally, the presence of openings is also shown to have statistically relevant impact on the level of interstory drift ratio triggering the lower damage states.

1. INTRODUCTION

Masonry infills are one of the most prevailing types of non-structural elements in buildings of both Western and Eastern modern architecture. As witnessed by reconnaissance missions and surveys after recent strong seismic events (L'Aquila, Italy, 2009 [1], Maule, Chile, 2010 [2,3], Muisne, Ecuador, 2016 [4]), damage to non-structural components and particularly infills often account for most of the earthquake induced economic losses. This is due because, on the one hand, non-structural components typically represent a large portion (from 70% to 90%) of the total cost of buildings and, on the other hand, because their damage is generally triggered at levels of structural response that are typically much lower than those required to initiate structural damage [5]. Therefore, far more nonstructural damage than structural damage is usually observed as a result of earthquakes.

Nonstructural masonry infill walls are commonly used for exterior enclosures as well as for interior partitions in low to mid-rise reinforced concrete (RC) or steel frame buildings. They are typically made of either solid or hollow clay or concrete bricks, joined with cement or lime mortar. Generally, these panels are very stiff in their plane and exhibit a relatively brittle behavior. Even though a large number of studies have been conducted on masonry infill walls, the large majority of these studies have focused on improving our understanding of their lateral strength and seismic response primarily by evaluation of their measured hysteretic behavior. Nevertheless, there is only a limited number of contributions that have attempted to estimate the level of damage as a function of the level of lateral deformations.

Fig. 1 depicts a couple of photographs of buildings in Ecuador after the 2016 earthquake, which illustrate examples of in-plane failure of exterior and interior masonry infill walls, making evident the possible consequences to life safety arising from failure of these elements, in addition to downtime and economic losses. It should be also pointed out that partial or total out-of-plane collapse of masonry infill walls (see also [6]) is, in most cases, preceded by in-plane cracking and crushing at the corners. Thus, an in-depth characterization of in-plane damage in masonry infills undergoing lateral displacements is of utmost importance not only to estimate in-plane damage per-se, but also to estimate the likelihood of experiencing an out-of-plane failure.

Most of current seismic codes are force-based and, therefore, primarily rely on checking that structural elements have sufficient strength and give secondary importance to lateral deformations and to the performance of nonstructural components [7]. For this reason, whilst an important body of work has addressed the assessment of the strength of masonry infill walls and their influence on building response, very few studies have been devoted to estimating the progression of in-plane damage as a function of lateral deformations being imposed on them (see e.g. [8]).

Recently, there has been an increasing interest in performance-based seismic assessment procedures [9,10], which are aimed at estimating the seismic risk of man-made facilities taking into account all potential sources of uncertainty. In the Performance-Based Earthquake Engineering (PBEE) framework developed by the Pacific Earthquake Engineering Research (PEER) Center, seismic performance is quantified in terms of one or more decision variables. This fully probabilistic framework explicitly takes into account uncertainties in the seismic hazard, seismic response, damage estimation and risk estimation and allows these uncertainties to be propagated and rationally accounted for. For example, based on the PEER-PBEE framework, Aslani and Miranda [11] developed a building-specific loss estimation methodology in which the expected annual loss (EAL) is computed as the sum of expected losses in each component at a given level of ground motion intensity and then integrating over the mean annual frequencies of exceeding of all possible intensities. Therefore, the EAL can be computed as follows:

$$EAL = \int_0^{\infty} \sum_{j=i}^{n} E\left[L_j \mid IM = im\right] \left| \frac{d\nu(IM = im)}{d(IM)} \right| d(IM) \tag{1}$$

where

$$E\left[L_j \mid IM = im\right] = \int_0^{\infty} \sum_{i=1}^{m} E\left[L_j \mid DS = ds_i\right] P\left[DS = ds_i \mid EDP_j = edp\right] dP\left[EDP_j > edp \mid IM = im\right]. \tag{2}$$

In Eq. (2), $E[L_j \mid DS = ds_i]$ is the conditional expectation of the loss in the *j*-th component given that it has reached damage state ds_i, whereas $P[DS = ds_i \mid EDP_j = edp]$ is the conditional probability that the *j*-th component will reach or exceed damage state ds_i when undergoing an engineering demand parameter (*EDP*) equal to *edp*; *n* is the total number of components whereas *m* is the total number of damage states considered. Furthermore, $P[EDP_j > edp \mid IM = im]$ is the exceedance conditional probability of the engineering demand parameter *edp* at an intensity measure (*IM*) level reaching the value *im* and $\nu(IM = im)$ is the mean annual frequency of exceedance of $IM = im$, that is, the ordinate of the site-specific seismic hazard curve at $IM = im$. In Eq. (2), $P[DS = ds_i \mid EDP_j = edp]$ is what is commonly referred to as the fragility function, which provides information on the probability of reaching or exceeding various damage states at increasing levels of building response, for example at increasing levels of peak interstory drift.

It should be noticed that, in Eq. (1) and (2), the convention indicating random variables with upper case letters and specific values assigned to them with lower case letters has been adopted.

Fig. 1 Masonry infills damaged after the Ecuador 2016 earthquake (photos by E. Miranda).

It is well known that, after earthquakes, most of the damage produced in buildings is the result of lateral deformation demand imposed on the structure by the ground motion shaking. For this reason, in modern performance-based seismic assessment approaches, damage estimation to most structural and nonstructural components is done as a function of interstory drift demands. From Eq. (1), it is then clear that most recent performance assessment methodologies rely on the availability of fragility functions. For instance, Aslani and Miranda [12] developed drift-based fragility curves for slab-column connections in non-ductile RC structures. Similarly, Ruiz-Garcia and Negrete [13] proposed drift-based fragility curves for confined masonry walls.

Despite several dozen experimental studies on the testing of masonry infill walls, most of them has been aimed at determining strength, stiffness and modeling criteria. However, there is very little research specifically focused on developing drift-based fragility functions for masonry infills, which, as previously discussed, are of paramount importance to estimate damage to these elements.

Two notable exceptions are the recent works by Cardone and Perrone [14] and Sassun et al. [15] who, to the best of our knowledge, developed the first drift-based fragility functions for masonry infill walls. Cardone and Perrone gathered and analyzed the experimental results of 19 different studies for a total of 55 specimens. They subdivided their specimens into two groups, masonry infill walls, either exterior or interior, without openings and those with openings. For each of the two groups they developed drift based fragility curves for four damage states ranging from light diagonal cracking to global collapse of the infill. As expected, they found higher vulnerability in infill walls with openings. More recently, Sassun et al. [15], considered experimental results of 14 studies for a total of 50 specimens. They defined four damage states very similar to the ones presented in [14] but, differently from [14], they only provided fragility curves for the whole sample without considering the effects due to the presence of openings. In addition to that, they conducted a relatively simple investigation on the effects of the type of masonry on the fragility of the infill walls. No other variable, which might influence the fragility of masonry infills, was taken into consideration.

Although both of these studies are extremely valuable, they are based on a relatively small sample, especially when subdividing the dataset into subgroups for evaluating the influence of type of masonry or the presence of openings. Furthermore, limited statistical analyses were conducted to determine which are the main variables that lead to statistically significant fragilities.

The aim of the present paper is to develop drift-based fragility functions relying on a wide and up-to-date collection of experimental results contained in literature on in-plane loaded infilled frames. Three damage states have been suitably defined, strictly related to the repair/replacement actions required as a result of the damage state to facilitate their use in probabilistic performance-based seismic assessment and earthquake-induced loss estimation.

For that purpose, a large database has been built containing information on lateral drift levels associated to the three damage states for 152 masonry infilled frame specimens when subjected to lateral cyclic loading. Then, drift-based fragility functions have been developed, by carefully analyzing the influence of the type of brick or masonry unit employed, mortar compressive strength, masonry prism compressive strength and the presence of openings. Also, specimen-to-specimen and finite sample uncertainty have been quantified. In particular, bi-variate fragility functions (i.e. fragility surfaces) taking into account both interstory drift ratio and mortar or masonry prism compressive strength have been obtained.

It should be noted that the empirical fragility functions developed in this study are based on the results of experimental testing of specimens with only in-plane loading and therefore do not account for out-of-plane loading, which several studies have shown may be important (e.g. [16,17]). However, in most cases, out-of-plane failure is preceded by in-plane damage to the infill. Thus, the information contained in this paper provides useful tools to estimate in-plane damage to masonry infill walls.

2. DAMAGE STATE DEFINITION

In the present study, three discrete damage states are proposed in order to describe the evolution of damage in masonry infills undergoing earthquake-type in-plane loading and derive their corresponding fragility functions. Three damage states are defined after the damage patterns observed both in infilled frames tested experimentally, undergoing lateral cyclic loading, and after reconnaissance missions in buildings struck by major seismic events. Furthermore, it is desirable that damage states correspond to those requiring different repair actions. In fact, the identification, for each damage state, of the interventions required to repair the damaged infill is pivotal to the estimation of expected earthquake-induced economic losses in the PBEE framework. For these reasons, although it is possible to define a greater number of damage states (and several attempts can be found in literature, see e.g. [18]), they would imply a finer distinction among required repair interventions which is actually impractical and in some cases meaningless. Furthermore, experimental studies available in literature most often only report information (i.e., damage pattern and corresponding lateral drift) related to the aforementioned damage states.

2.1 Damage State 1 (DS_1)

This damage state corresponds to the initiation of small hairline cracks in masonry, up to 2mm wide, mainly concentrated in bed and head joints, in plaster (when present) or along the interfaces with the columns and/or the top beam of the frame.

No significant joint sliding and crushing of the units is observed. This damage state requires only very light and simple repair interventions. Typical repair action consists in locally plastering the visible cracks and applying new painting. A couple of examples of infills showing a DS_1 damage are depicted in Fig. 2.

2.2 Damage State 2 (DS_2)

This damage state corresponds to the beginning of significant cracks, more than 2mm wide, propagating through both mortar joints and masonry blocks with possible but very limited sliding between joints and localized crushing of units (for example at the corners). Heavier interventions are required to repair an infill in this damage state. Typical repair actions consist in the removal of the old plaster, demolition of broken bricks, local reconstruction of masonry, application of a new higher quality plaster coat and new painting. Examples of infills showing a DS_2 damage state are depicted in Fig. 3.

Fig. 2 Masonry infills displaying DS_1 damage state observed after the Ecuador 2016 earthquake (photos by E. Miranda).

Fig. 3 Masonry infills displaying DS_2 damage state observed after the Ecuador 2016 earthquake (photos by E. Miranda).

Fig. 4 Masonry infills displaying a DS_3 damage observed after the Ecuador 2016 earthquake (photos by E. Miranda).

2.3 Damage State 3 (DS_3)

This damage state corresponds to the development of wide diagonal cracks (usually larger than 4mm) with significant sliding between joints and widespread crushing and spalling of masonry units. Repairing the panel is not economically convenient and, therefore, complete demolition and subsequent reconstruction are advised. Examples of infills showing a DS_3 damage state are depicted in Fig. 4.

3. DESCRIPTION OF COLLECTED DATA

Estimation of the probability of observing a given damage state in a masonry infill after an earthquake requires gathering statistical information about the level of lateral deformation at which that damage state has occurred. Ideally, the use of information from actual buildings hit by seismic actions, exhibiting different level of damage would be desirable. However, the interstory drift ratio (*IDR*) that produced the observed damage at various floor levels is, in most cases, unknown. Therefore, in this study, experimental results from 152 specimens of masonry infilled RC or steel frames, tested under lateral cyclic loading were collected from literature in order to infer the required statistical information about the lateral displacement capacity of masonry infills. A careful interpretation of the data collected allowed to determine the *IDR* for which each specimens experienced the onset of one or more of the damage states defined in the previous Section. Whereas a very large amount of data is available in the literature, many of the existing experimental reports on masonry infills do not contain enough information for the purposes of this study and only a selected subset of them can be actually employed for associating a value of lateral displacement to the onset of each damage state here defined. For these reasons, data from 33 experimental research programs conducted over the last 32 years were considered, in which specimens were not excessively scaled in size and a description of the damage was provided with sufficient detail at various stages of testing. Complete experimental force-displacement responses for the laterally loaded infilled frames were also provided. Three different kind of masonry units, corresponding to the most prevailing types actually employed in the construction practice, were used for the infill specimens analyzed: solid clay bricks, hollow clay bricks and concrete masonry units. Infill specimens with the presence of openings were also included. In addition to the drift levels at which one or more of the defined damage states occurred, information about measured compressive strength for both mortar and the masonry prism, the dimensions of the panel and the presence of openings were also compiled. It was not always possible to detect, for each specimen, the lateral displacement level for all the three damage states, either because the damage state did not occur or, especially for older experimental programs, because the report did not document well enough the needed information. The latter situation was more common for the first two damage states mainly because, until recently, earthquake provisions were primarily involved with life safety rather than damage control. A careful study of experimental investigations systematically reporting crack patterns and crack widths at various drift levels (e.g. [19,20]) suggested that, in a significant number of cases, the first damage state occurs at the drift corresponding to the first reduction of lateral stiffness in the elastic range of the force-displacement response curve. Moreover, the second damage state is usually observed when the specimen reaches its maximum lateral load capacity. This evidence could be used to expand the number of data points, based on the analysis of the force-displacement curves only. Nevertheless, since, in general, the force-displacement curve also reflects the contribution of the external frame behavior (especially in the case of RC frames), for masonry infills the procedure is not straightforward and can be misleading. Furthermore, many of the testing reports did not provide enough details of the surrounding framing elements.

Ref.	# Spec.	Scale	Masonry Unit	Mortar CS f_m [MPa]	Prism CS f_p [MPa]	Thickness t [m]	Length L [m]	Height H [m]	Openings
[21]	1	1:2 RC	HCB	4.3	n.d.	0.080	2.415	1.635	w/o
[22]	2	1:2 RC	HCrB(1)-SCB(1)	10.5	18.1-26.7	0.06-0.1	1.829	1.327	w/o
[23]	5	1:1 RC	SCB	6.2-8.3	3.5-11.0	0.047-0.187	2.438	1.626	w/o
[24]	9	1:2 RC	SFB	17.3	3.9-4.6	0.055-0.110	1.500	1.500	w/o
[25]	1	1:2 RC	HCB	11.7	V=6.2; H=2.9	0.120	2.300	1.300	w/o
[26]	1	1:1 RC	HCB	5.5	1.1	0.115	4.200	2.750	w/o
[27]	2	1:1 RC	SCB	7.0	8.4	0.200	3.2-6.8	2.640	w/o
[28]	10	1:2 RC	HCB	10.4-25.1	V=2.2-5.1; H=2.5-3.9	0.120-0.160	1.7-2.3	1.300	w/o
[29]	2	3:4 RC	SCrB	8.0	19.3	0.090	2.516	2.000	w/o
[30]	1	1:1 RC	HCB	19.9	n.d.	0.300	4.450	2.680	w/o
[20]	12	1:1 RC	HCrB	12.4-24.4	17.4-35.4	0.200	3.600	2.800	w/o
[31]	9	1:1 S	HCB	medium	V=2.3-5.6; H=2.6-4.1	0.195-0.330	2.2-7.3	2.2-6.2	w/o
[32]	10	1:2 RC	HCB(4)-SCB(6)	0.5-5.1	3.5-5.2	0.12	1.85	1.3	w/o
[33]	1	n.d.	HCrB	n.d.	n.d.	0.150	2.400	1.550	w/o
[34]	2	1:1 RC	HCB	11.7-18.7	11.4-17.4	0.089	2.007	2.070	w/o
[35]	6	1:1 RC	ACB	3.1	3.5	0.200	5.240	2.725	w/o
[19]	9	1:3 RC	HCB	1.5	V=2.6 H=5.1	0.093	1.200	0.800	w/o(1) -w(8)
[36]	2	1:4 RC	SCB	n.d.	n.d.	0.060	0.900	0.700	w/o(1)-w(1)
[37]	10	1:3 S	HCrB	18.0	10.0	0.067	1.1-1.7	1.080	w/o(8)-w(2)
[38]	5	1:2 RC	SCB	8.3	2.3	0.106	2.100	1.300	w/o(1) -w(4)
[39]	9	1:2 S	HCB(3)-ACB(6)	5.0	1.0-2.0	0.125-0.190	2.062	1.556	w/o
[18]	10	1:2 RC	HCrB (4)-SCrB(6)	15.0	9.5-15.1	0.092	2.057	1.422	w/o
[40]	2	1:2 RC	HCB	medium	n.d.	0.120	2.000	1.250	w/o
[41]	1	1:1 RC	HCB	7.7	4.6	0.350	4.220	2.950	w/o
[42]	3	1:4 S	HCB	11.7-21.4	16.5-22.8	0.100	1.800	0.940	w/o(1)-w(2)
[43]	1	1:1 S	HCB	12.2	7.1	0.190	2.930	2.460	w/o
[44]	1	1:1 RC	SCB	10.0	n.d.	0.092	6.100	3.050	w/o
[45]	1	1:2 S	SCB	28.0	4.5	0.130	2.100	1.650	w/o
[46]	5	1:1 S	SCB	low	5.3-7.3	0.1-0.2	2.740	1.676	w
[47]	9	1:2 RC	HCB	5.2	2.7	0.120	2.000	1.400	w/o(1)-w(8)
[48]	5	1:1 S	SCB	10.1	7.0-8.5	0.110	2.260	1.800	w/o(1)-w(4)
[49]	3	1:2 RC	HCB	10.0	15.2	0.120	2.080	1.500	w/o
[50]	2	1:2 RC	HCB	5.0-5.1	1.9-4.3	0.120	1.800	1.300	w/o

SCB: Solid Clay Bricks; HCB: Hollow Clay Bricks; HCrB: Hollow Concrete Blocks; SCrB: Solid Concrete Blocks; ACB: Aerated Concrete Blocks; RC: Reinforced Concrete; S: Steel; CS: Compressive Strength; V: Vertical compr. strength; H: Horizontal compr. strength.

Table 1. Summary of the experimental data for masonry infilled frames with in-plane loading used in this study.

For these reasons, in the present study only data with a sufficiently precise visual description were included. Table 1 summarizes the main features of each experimental research program considered. Given its dimensions, an extended table containing the *IDR* levels for the onset of damage states for each specimen is provided as an electronic supplement available through the Stanford Library website.

4. FRAGILITY FUNCTIONS

The *IDR* at which each damage state was observed in the masonry infilled specimens exhibits relatively large variability from one specimen to another. This specimen-to-specimen variability can be explicitly accounted for by developing drift-based fragility functions estimating the likelihood that a given infill panel reaches or exceeds a certain damage state conditional on a given peak *IDR*. The experimental dataset summarized in Table 1 is used for developing fragility functions for each of the three damage states defined in Section 3, as well as evaluating the influence of other factors such as the type of masonry block employed, mortar and masonry compressive strength, presence of openings and epistemic uncertainty due to the limited number of specimens. Diagonal compression or shear tests of the masonry were only reported in a small number of the experimental programs, and therefore it was not possible here to evaluate its influence on the fragility of the infills. Similarly, an attempt was made to evaluate the influence of the aspect ratio of the masonry infills, however many of the specimens had similar aspect ratios and the range of aspects ratios was not very large, so it was found not to be statistically significant for this database.

For each damage state, a cumulative frequency distribution is obtained by plotting interstory drift ratios IDR_i at which the damage state was experimentally observed, sorted in ascending order, against the plotting probability F_i defined by the following relation:

$$F_i = (i - 3/8)/(N + 1/4) \tag{3}$$

where i is the rank of the IDR_i after sorting and N is the number of specimens. The relation represented by Eq. (3), proposed in [51], has been proven to provide unbiased plotting positions [52].

In order to build fragility functions, a probability density function must be chosen which adequately fits the obtained experimental cumulative frequency distribution. A number of distributions have been proven to be suited for this purpose, but the log-normal distribution is a common choice in engineering applications when the values of the random variable are known to be strictly positive, as in the present study. Moreover, when compared to other skewed probability distributions (as, for instance, Gumbel or Weibull) log-normal distribution has the advantage of being quite commonly used for fragility functions. Its probability distribution is fully defined by only two statistical parameters, as follows:

$$P(DS \geq ds_i \mid IDR = \delta) = 1 - \Phi\left(\frac{\ln(\delta) - \mu_{\ln(\delta)}}{\beta}\right) \tag{4}$$

where $P(DS \geq ds_i \mid IDR = \delta)$ is the conditional probability of reaching or exceeding a certain damage state ds_i in the masonry infill at a specific *IDR* value equal to δ. $\mu_{\ln(\delta)}$ and β represent the central tendency and the dispersion parameters of the cumulative standard normal distribution Φ. The two parameters characterizing the log-normal distribution are estimated according to the method of moments (see, e.g., [53]) which, given the number of specimens constituting the sample, provides a good fit of the distribution to the data points. Thus, central tendency and dispersion parameters $\mu_{\ln(\delta)}$ and β are estimated as the mean and the standard deviation of the logarithm of *IDR*s of the sample data, respectively. Table 2 contains the statistical parameters for the fitted lognormal probability distribution for each damage state and the number of specimens for each sample. In particular, $\mu_{\ln(\delta)}$ and β parameters have been included, as well as the geometric mean $\overline{IDR} = \exp(\mu_{\ln(\delta)})$, which is especially useful to readily visualize the *IDR* value having a 50% probability of reaching or exceeding the given damage state.

Damage State	$\overline{IDR}$ [%]	$\mu_{\ln(\delta)}$	β	Number of Specimens
DS_1: light cracking	0.125	-2.078	0.325	100
DS_2: moderate cracking	0.327	-1.118	0.278	118
DS_3: heavy cracking	0.820	-0.198	0.320	132

Table 2. Statistical parameters estimated for interstory drift ratios corresponding to the three damage states in masonry infills.

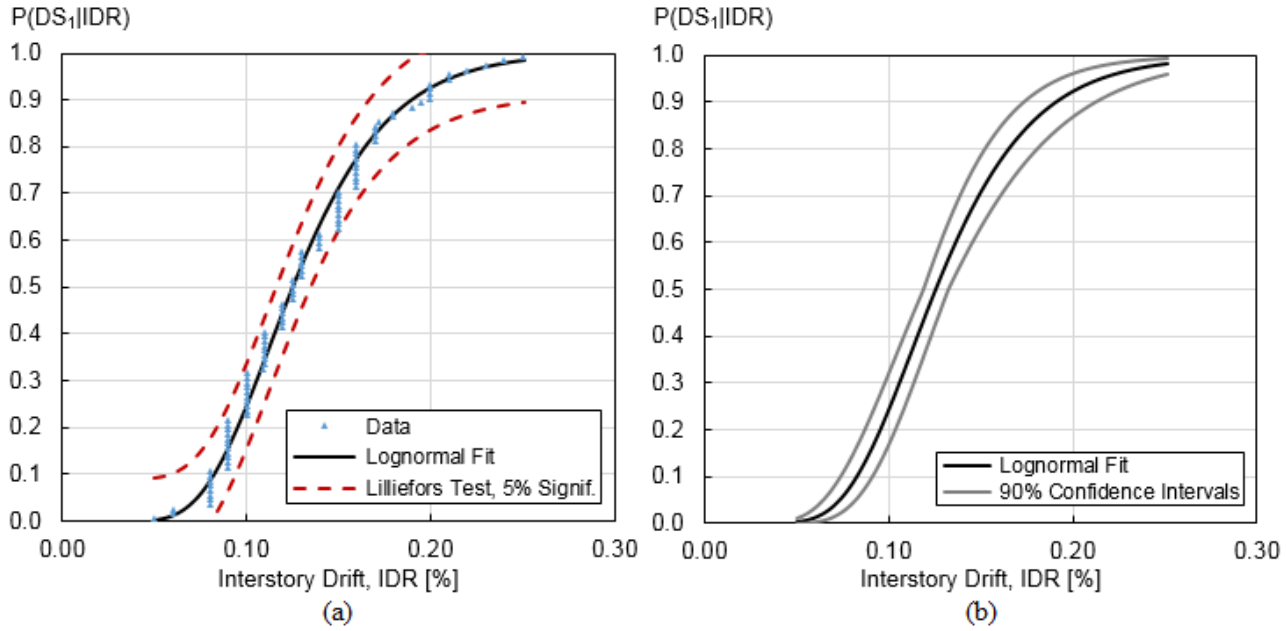

Fig. 5 (a) Fragility function fitted to interstory drift ratios corresponding to damage state DS_1 in masonry infills. (b) Incorporating finite-sample uncertainty to the DS_1 fragility function.

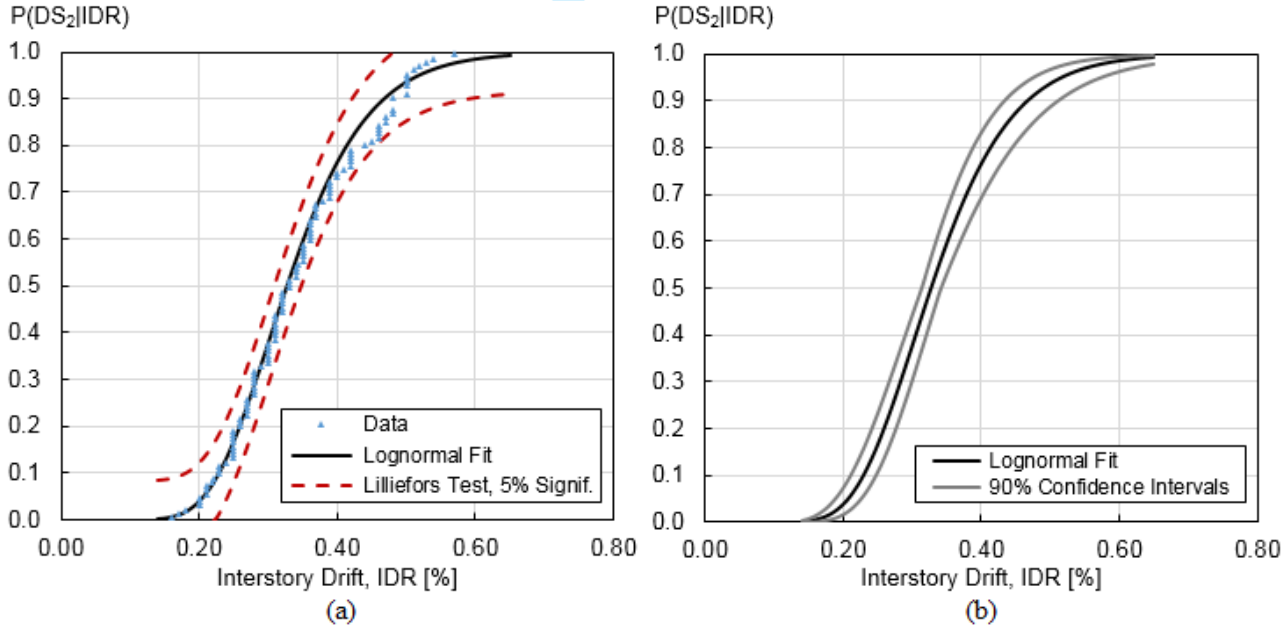

Fig. 6 (a) Fragility function fitted to interstory drift ratios corresponding to damage state DS_2 in masonry infills. (b) Incorporating finite-sample uncertainty to the DS_2 fragility function.

From Table 2, *IDR* values having a 50% probability of inducing damage states DS_1, DS_2 and DS_3 in infilled walls are equal to 0.125%, 0.327% and 0.820% respectively. The log-normal fitting has been carried out under the null hypothesis that the difference between the actual cumulative distribution function of the sample and the estimated standard log-normal distribution is not statistically significant at every point. In order to verify that the above null hypothesis cannot be rejected, a Lilliefors goodness-of-fit test at 5% significance level was conducted for each fragility function. This test is based on the Kolmogorov-Smirnov goodness-of-fit test and is used when the parameters describing the hypothesized distribution are not known for the population but rather are inferred from the sample (see [54]), as is the case of the present study. Fig. 5 (a), Fig. 6(a) and Fig. 7(a) depict, for each of the three damage states, the empirical cumulative distributions of observed data, the proposed fragility functions obtained through log-normal fit (whose parameters are reported in Table 2), and a graphical representation of the Lilliefors test. It can be seen that, for each damage state, the lognormal probability distribution provides a reasonable characterization of the empirical distribution.

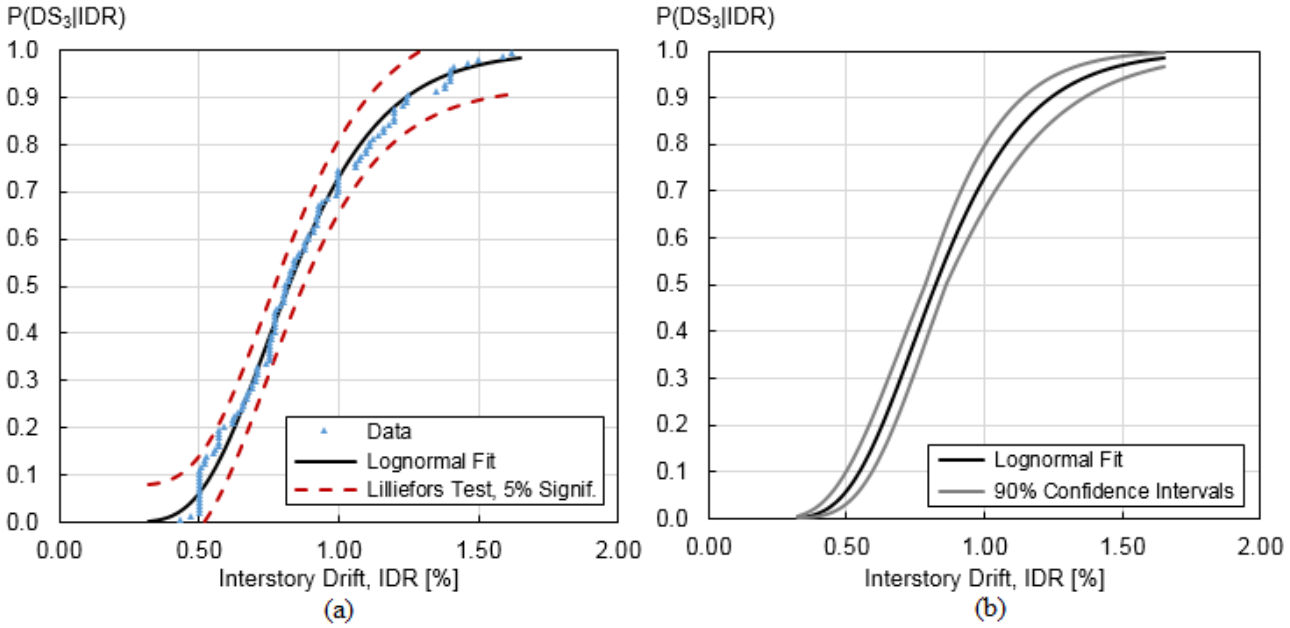

Fig. 7 (a) Fragility function fitted to interstory drift ratios corresponding to damage state DS_3 in masonry infills. (b) Incorporating finite-sample uncertainty to the DS_3 fragility function.

4.1 Influence of finite-sample uncertainty

The dispersion parameter β, accounting for the specimen-to-specimen variability and reported in Table 2, is very similar for each of the damage states. Nevertheless, the additional uncertainty arising from the parameters defining the proposed fragility functions being estimated from a limited number of specimens must be evaluated. This source of epistemic uncertainty is known as finite-sample uncertainty. A quantitative measure for this type of uncertainty can be provided by computation of the confidence intervals for each of the statistical parameters defining the assigned fragility function. Since the underlying probability distribution is lognormal, confidence intervals for the logarithmic mean and standard deviation $\mu_{\ln(\delta)}$ and β can be obtained from a conventional approach. In particular, the confidence interval for the mean of a lognormally distributed sample of *n* data points can be obtained through the following expression [55]:

$$\mu_{ln(\delta)} \pm t_{\alpha/2,n-1} \frac{\beta}{\sqrt{n}}, \tag{5}$$

where $t_{\alpha/2,n-1}$ is the *t*-distribution for $n-1$ degrees of freedom, the probability of exceeding which is $P(t)=\alpha/2$. Unlike the confidence limits for the mean, which are symmetric about the estimate $\mu_{\ln(\delta)}$, confidence limits for the logarithmic standard deviation are non-symmetric and can be approximated as follows [55]:

$$\left[\frac{(n-1)\beta^2}{\chi^2_{\alpha/2,n-1}}\right]^{1/2} \quad \text{and} \quad \left[\frac{(n-1)\beta^2}{\chi^2_{1-\alpha/2,n-1}}\right]^{1/2}, \tag{6}$$

where $(n-1)\beta^2 = \sum \left(\ln(\delta_i) - \mu_{\ln(\delta)}\right)^2$ and $\chi^2_{\alpha/2,n-1}$ is the inverse of the χ^2 distribution with $n-1$ degrees of freedom and a probability of occurrence of $\alpha/2$. Analogously, $\chi^2_{1-\alpha/2,n-1}$ is the inverse of the χ^2 distribution with $n-1$ degrees of freedom and a probability of occurrence of $1-\alpha/2$.

By employing Eqs. (5) and (6) lower and upper confidence intervals for $\mu_{\ln(\delta)}$ and β are computed and used to draw a confidence band around the original fragility curve.

Fig. 5(b), Fig. 6(b) and Fig. 7(b) depict, for each fragility curve, the computed confidence intervals at a 90% significance level. In these figures, the black line corresponds to the fragility function in the absence of finite-sample uncertainty whereas gray lines delimit the 90% confidence band due to this source of epistemic uncertainty. The corresponding upper and lower bounds for statistical parameters are reported in Table 3. As shown in the proposed figures, the influence of finite-sample uncertainty is significant and needs to be taken into account when performing sensitivity studies in loss estimations.

4.2 Influence of brick type

Fragility curves portrayed in Fig. 5, Fig. 6 and Fig. 7 were obtained by considering all 152 specimens without taking into account the possible effects of brick type, material properties or geometry. In particular, it should be of interest to investigate if brick type has any significant influence on the likelihood of attaining a certain damage state.

To this aim, Fig. 8 portrays a plot of the *IDR*s at which each specimen experiences damage states DS_1 and DS_3. A quick look at the dispersion graphs shown in Fig. 8 suggests that information on brick type alone do not introduce any significant improvement on the dispersion of the original fragility functions described in the previous Subsections.

In order to ascertain this conjecture, all specimens have been grouped into three dataset corresponding respectively to masonry infills made with solid clay bricks, hollow clay bricks and concrete masonry units. For each group of specimens, the logarithmic mean $\mu_{\ln(\delta)}$ and the logarithmic dispersion β have been computed, which allow to obtain fragility functions for each of the three datasets.

Two-sample *t*-tests have been conducted to establish if the logarithmic means of the three samples are significantly different from each other, or, in other words, if the type of brick makes a significant difference in the fragility of the masonry infill. Because, as shown in Fig. 8, there is considerable variability in the *IDR*s producing DS_1 and DS_3 for any of the three types of bricks, then simply computing a difference in their logarithmic mean values does not necessarily implies that the brick type makes a significant difference. Since each value of a given dataset is sampled independently from each other and the population is log-normally distributed, the *t*-test can be applied to evaluate whether a null-hypothesis ("brick type does not make a significant difference") can be accepted or must be rejected.

Given two datasets, for example the group of solid clay infills and the group of hollow clay infills, with logarithmic means $\mu^1_{\ln(\delta)} = \mu_1$ and $\mu^2_{\ln(\delta)} = \mu_2$, logarithmic standard deviation β_1 and β_2, and number of specimens n_1 and n_2 respectively, the first step consists in computing the statistics which is simply the difference between means $\Delta\mu = \mu_1 - \mu_2$. Therefore, the null hypothesis to be tested is that $\Delta\mu = 0$.

Damage State	$\overline{IDR}$ *range* [%]	$\mu_{\ln(\delta)}$	β
DS_1: light cracking	0.119 ÷ 0.132	-2.078 ± 0.054	0.325 ± 0.043
DS_2: moderate cracking	0.314 ÷ 0.341	-1.118 ± 0.042	0.278 ± 0.034
DS_3: heavy cracking	0.784 ÷ 0.859	-0.198 ± 0.046	0.320 ± 0.037

Table 3. 90% confidence intervals: statistical parameters estimated to incorporate epistemic uncertainty due to finite-sample for interstory drift ratios corresponding to the damage states in masonry infills.

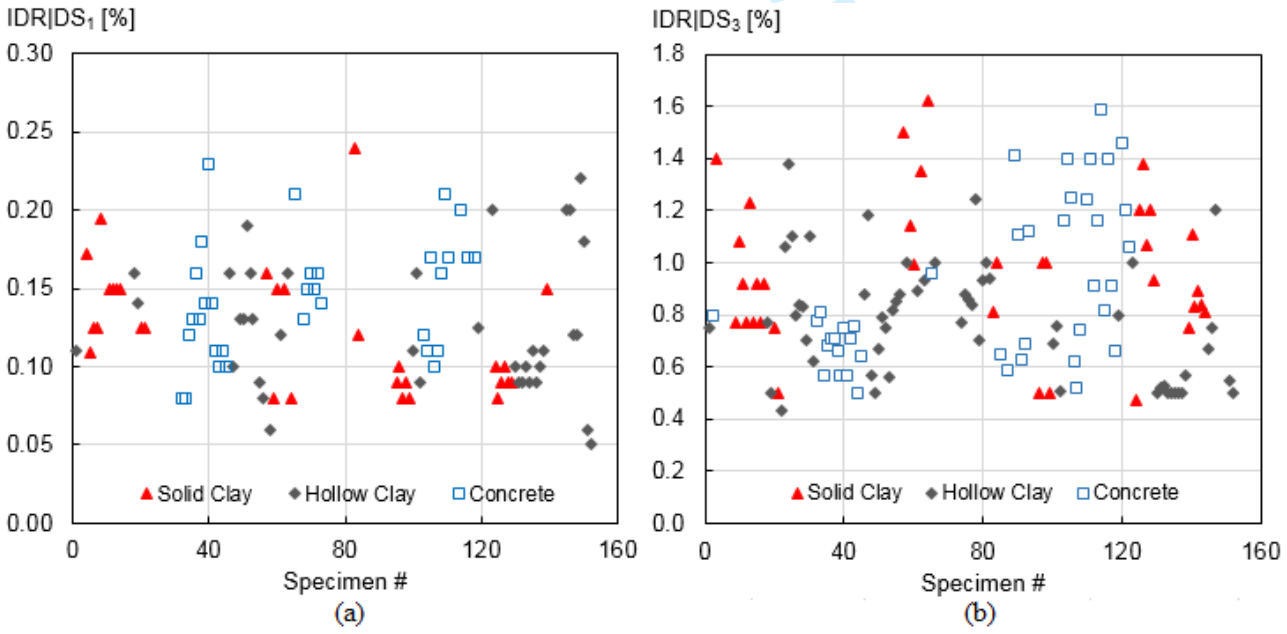

Fig. 8 Interstory drift ratio at which each specimen reaches damage states DS_1 (a) and DS_3 (b) respectively.

The sum of squares error can be computed as follows:

$$SSE = \sum_{j=1}^{n_1}\left(\ln(\delta_j) - \mu_1\right) + \sum_{j=1}^{n_2}\left(\ln(\delta_j) - \mu_2\right). \quad (7)$$

Given that the number of degrees of freedom df is equal to $(n_1 - 1) + (n_2 - 1)$ it is possible to define the mean square error as:

$$MSE = SSE / df. \quad (8)$$

Finally, the estimate for the standard error of the statistics can be computed as follows:

$$s_{\mu_1 - \mu_2} = \sqrt{\frac{2MSE}{n_h}}, \quad (9)$$

where n_h is the harmonic mean of the sample sizes, computed as $n_h = 2/(1/n_1 + 1/n_2)$. It is now possible to compute the t-distribution value corresponding to the following statistic:

$$t^* = \frac{\mu_1 - \mu_2}{s_{\mu_1 - \mu_2}} \quad (10)$$

Finally, knowing the number of degrees of freedom df, the probability of getting a t as large or larger than t^* or small or smaller than $-t^*$ (for a two-tailed test) can be obtained. If the computed probability is less or equal to the significance level, here chosen equal to 5%, the null hypothesis must be rejected and the difference in means between the two different groups is considered statistically significant.

Table 4 contains statistical parameters for the lognormal distribution governing fragility functions for the three groups of specimens at each of the three damage states.

Nevertheless, as summarized in Table 5, which reports the outcome of the t-tests, the difference between means of each pair of the three datasets turns out to be not statistically significant for five pairs of datasets out of the nine possible pairs (resulting from having three types of bricks and three damage states). This means that the brick type, per se, in general does not always has an impact on the fragility function of a masonry infill.

	DS1: Light Cracking			DS2: Moderate Cracking			DS3: Heavy Cracking		
Brick Type	$\mu_{\ln(\delta)}$	β	# Spec.	$\mu_{\ln(\delta)}$	β	# Spec.	$\mu_{\ln(\delta)}$	β	# Spec.
Solid Clay	-2.139	0.300	30	-1.087	0.299	31	-0.127	0.262	35
Hollow Clay	-2.136	0.355	37	-1.146	0.301	50	-0.298	0.293	56
Concrete Units	-1.974	0.270	40	-1.104	0.221	34	-0.160	0.331	41

Table 4. Statistical parameters estimated for drift-based fragility functions corresponding to the three damage states in masonry infills for three different type of blocks.

	DS1: Light Cracking		DS2: Moderate Cracking		DS3: Heavy Cracking	
t-Test (brick type)	$\Delta\mu$	$P(\lvert t\rvert > t^*_{5\%})$	$\Delta\mu$	$P(\lvert t\rvert > t^*_{5\%})$	$\Delta\mu$	$P(\lvert t\rvert > t^*_{5\%})$
SCB vs HCB	0.003	**0.975**	0.058	**0.397**	0.171	**0.006**
SCB vs CrB	0.165	**0.027**	0.017	**0.795**	0.033	**0.631**
HCB vs CrB	0.162	**0.039**	0.041	**0.496**	0.137	**0.030**

Table 5. Results of the 5% significance level two-tailed t-tests on the difference between two logarithmic means for infills, considering three different types of masonry bricks and three damages states. Shaded cells indicate the cases for which the null hypothesis cannot be rejected (i.e. no significant difference between means).

One situation in which the type of brick produces a statistically significant difference is for damage state DS_1, where the type of brick has an influence on the tensile capacity of the brick. This is the case of concrete units, which require larger median deformation demands to initiate light cracking (DS_1) than those of clay bricks (either solid of hollow). Similarly, hollow clay bricks require smaller median deformation demands to produce DS_3, which involves heavier crushing and spalling, than those required in either solid clay or concrete bricks. As detailed in the following Subsection, it is expected that a more consistent and statistically significant influence on fragility is provided by measures of mortar or masonry prism compressive strengths.

4.3 Influence of mortar and prism compressive strength

In order to study whether the level of compressive strength for mortar f_m has some influence on the probability of exceeding a given damage state, the initial dataset has been subdivided into three subgroups according to mortar strength: infills with weak mortar, in which $f_m \le 5\,\text{MPa}$, infills with medium mortar strength, in which $5\,\text{MPa} < f_m \le 12\,\text{MPa}$, and infills with strong mortar, in which $f_m > 12\,\text{MPa}$. Fragility functions are computed through lognormal fitting for each dataset and for each damage state. Table 6 contains statistical parameters for the lognormal distribution governing fragility functions for the three subgroups of specimens at each of the three damage states.

Analogously to what was done in the previous Subsection for different brick types, two sample *t*-tests with 5% significance level have been carried out for each pair of datasets in each damage state, in order to assess if the difference in the means of each subgroup is statistically significant. A summary of the tests outcome is reported in Table 7.

From an analysis of the results, a significant dependence on mortar strength for damage states DS_1 is observed and, to a lesser extent, is also observed for DS_2. Fig. 9(a) depicts fragility curves for damage state DS_1 for the three levels of mortar strength. On the other hand, as shown in Table 7, damage state DS_3 is not significantly influenced by mortar strength. For DS_2, the influence of mortar strength is only significant for weak and medium levels of mortar strength. This suggests that the influence of mortar quality on the *IDR* at which a given damage state occurs, is smaller and less crucial as the damage level increases. A possible explanation is that, while at low damage levels the damage pattern involves significant cracking in the mortar (e.g., vertical and horizontal cracking between the infill and the frame, stepped cracking along bed and head joints), at higher levels of damage cracks primarily involve masonry units, with eventual crushing and spalling of the bricks. For this reason, it is interesting to investigate whether masonry prism compressive strength f_p, which accounts for the strength of both mortar and bricks, influences significantly the *IDR* for which all three damage states are attained by a given masonry infill. To this aim, the initial dataset has been subdivided according to prism compressive strength into two subgroups: infills with weak to medium prism strength, for which $f_p \le 5\,\text{MPa}$, and infills with medium to strong prism strength, for which $f_p > 5\,\text{MPa}$.

	DS_1: Light Cracking			DS_2: Moderate Cracking			DS_3: Heavy Cracking		
Mortar Strength	$\mu_{\ln(\delta)}$	β	# Spec.	$\mu_{\ln(\delta)}$	β	# Spec.	$\mu_{\ln(\delta)}$	β	# Spec.
Weak	-2.226	0.298	43	-1.266	0.293	37	-0.213	0.365	46
Medium	-2.077	0.333	35	-1.062	0.259	37	-0.175	0.287	39
Strong	-1.894	0.224	23	-1.036	0.223	42	-0.145	0.352	48

Table 6. Statistical parameters estimated for interstory drift ratios corresponding to the three damage states in masonry infills for three levels of mortar compressive strength.

	DS_1: Light Cracking		DS_2: Moderate Cracking		DS_3: Heavy Cracking	
t-Test (mortar)	$\Delta\mu$	$P(\lvert t\rvert > t^*_{5\%})$	$\Delta\mu$	$P(\lvert t\rvert > t^*_{5\%})$	$\Delta\mu$	$P(\lvert t\rvert > t^*_{5\%})$
W vs S	0.332	**0.001**	0.229	**0.001**	0.171	**0.361**
W vs M	0.149	**0.041**	0.204	**0.002**	0.033	**0.600**
M vs S	0.183	**0.015**	0.026	**0.642**	0.137	**0.663**

Table 7. Results of the 5% significance level two-tailed t-tests on the difference between two logarithmic means for infills, considering three different level of mortar compressive strength and three damages states. Shaded cells indicate the cases for which the null hypothesis cannot be rejected (i.e. no significant difference between means).

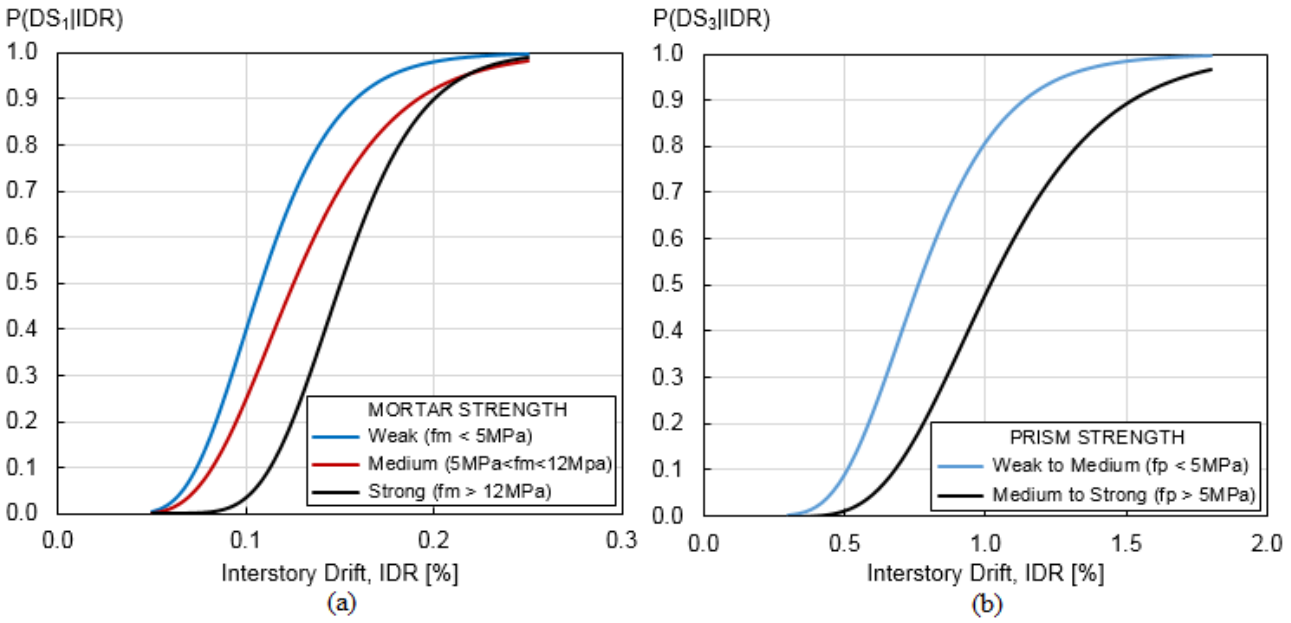

Fig. 9 (a) Fragility functions for masonry infills in damage state DS_1 with three different levels of mortar strength and (b) fragility functions for masonry infills in damage state DS_3 with two different levels of masonry prism strength.

Fragility functions are computed through lognormal fitting for the two dataset and for each damage state. Table 8 contains the statistical parameters for the lognormal distribution governing fragility functions for the two subgroups of specimens at each of the three damage states.

Again, in order to assess if the difference between their means is statistically significant, two sample *t*-tests with 5% significance level were carried out for the two datasets in each damage state. Results are summarized in Table 9. As it can be easily observed, compressive prism strength, as expected, influences significantly all three damage states. In particular, Fig. 9(b) depicts fragility curves obtained for damage state DS_3 and the two levels of prism compressive strength.

Based on results summarized in Tables 7 and 9, it can be concluded that, whereas mortar compressive strength primarily influences damage states with low level of damage and, therefore, can be employed to refine fragility functions for DS_1, prism compressive strength significantly influences all three damage states. Here we recommended its use to correct/improve fragility functions for DS_2 and DS_3, whenever information of the prism compressive strength of the infill is available.

	DS_1: Light Cracking			DS_2: Moderate Cracking			DS_3: Heavy Cracking		
Prism Strength	$\mu_{\ln(\delta)}$	β	# Spec.	$\mu_{\ln(\delta)}$	β	# Spec.	$\mu_{\ln(\delta)}$	β	# Spec.
Weak to Medium	-2.163	0.301	54	-1.187	0.292	52	-0.273	0.312	71
Medium to Strong	-1.974	0.375	29	-1.008	0.238	45	0.016	0.317	44

Table 8. Statistical parameters estimated for interstory drift ratios corresponding to the three damage states in masonry infills for two levels of compressive masonry prism strength.

	DS_1: Light Cracking		DS_2: Moderate Cracking		DS_3: Heavy Cracking	
t-Test (prism)	$\Delta\mu$	$P(\lvert t\rvert > t^*_{5\%})$	$\Delta\mu$	$P(\lvert t\rvert > t^*_{5\%})$	$\Delta\mu$	$P(\lvert t\rvert > t^*_{5\%})$
W vs S	0.190	**0.014**	0.178	**0.002**	0.289	**0.001**

Table 9. Results of the 5% significance level two-tailed t-tests on the difference between two logarithmic means for infills, considering two different level of compressive masonry prism strength and three damages states. The null hypothesis is rejected for all three cases.

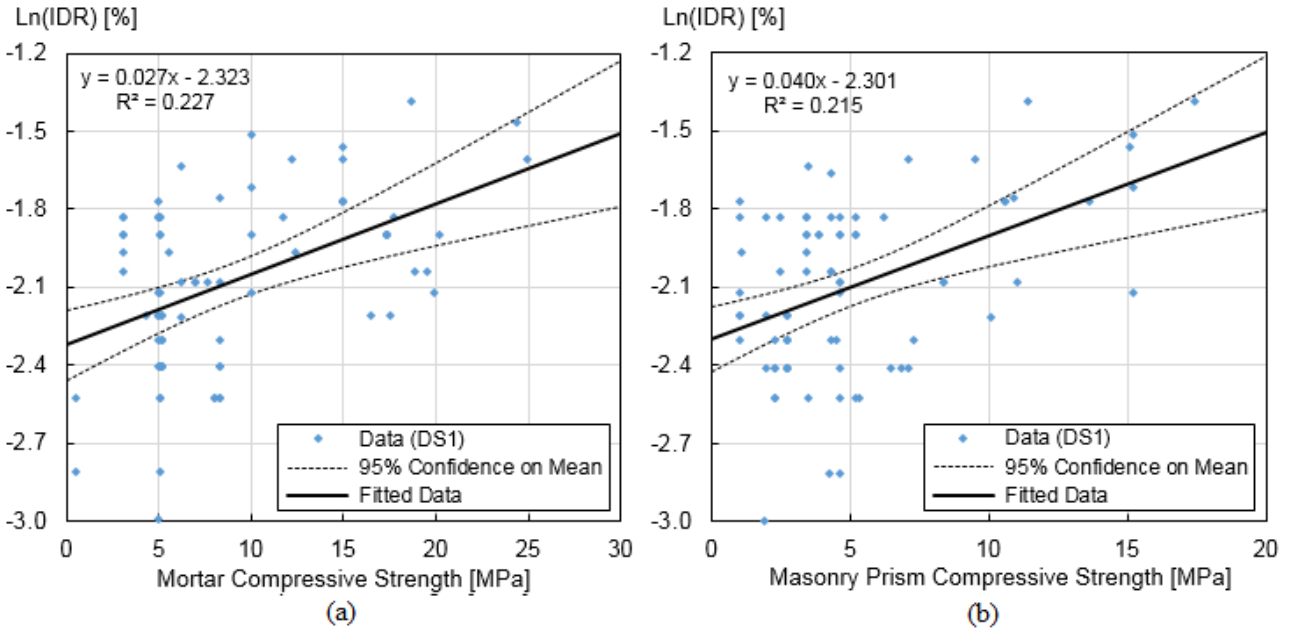

Fig. 10 Influence of mortar compressive strength (a) and prism compressive strength (b) on interstory drift ratios producing damage state DS_1.

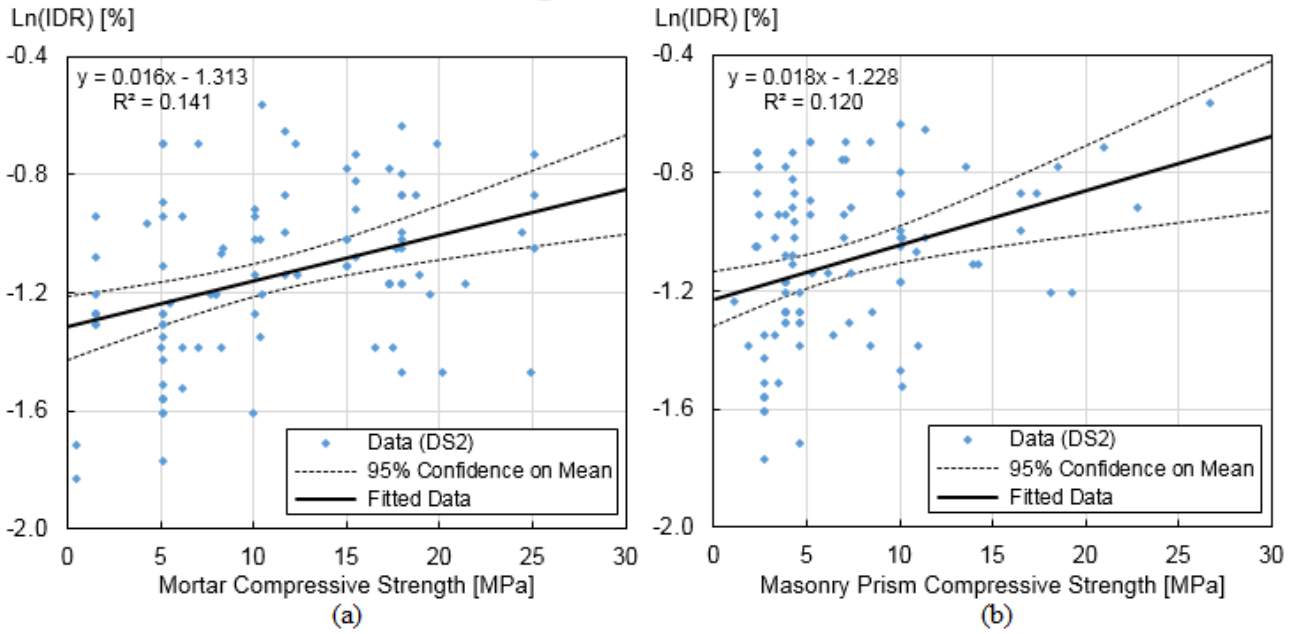

Fig. 11 Influence of mortar compressive strength (a) and prism compressive strength (b) on interstory drift ratios producing damage state DS_2.

Corroborated by the previous observations and based on the procedure first proposed by [11] for developing fragility surfaces, a more in-depth investigation is now proposed, which allows to explicitly account for the influence of mortar and prism compressive strength on fragility functions for masonry infills. More precisely, fragility surfaces, in which the probability of experiencing a given damage state is computed as a function of the *IDR* and mortar or prism compressive strength, are developed for cases in which this latter information or an estimate of it is available.

The influence of mortar compressive strength and prism masonry compressive strength on interstory drift ratios producing each of the three damage states is portrayed in Fig. 10, Fig. 11 and Fig. 12 respectively. In each case a linear regression of the *IDR* producing the damage state as a function of mortar compressive strength or masonry prism strength is shown. Coefficients (slope a_μ, y-intercept b_μ, and coefficient of determination R^2) are reported directly on the graph area, together with 95% confidence bands on the regressed linear fit.

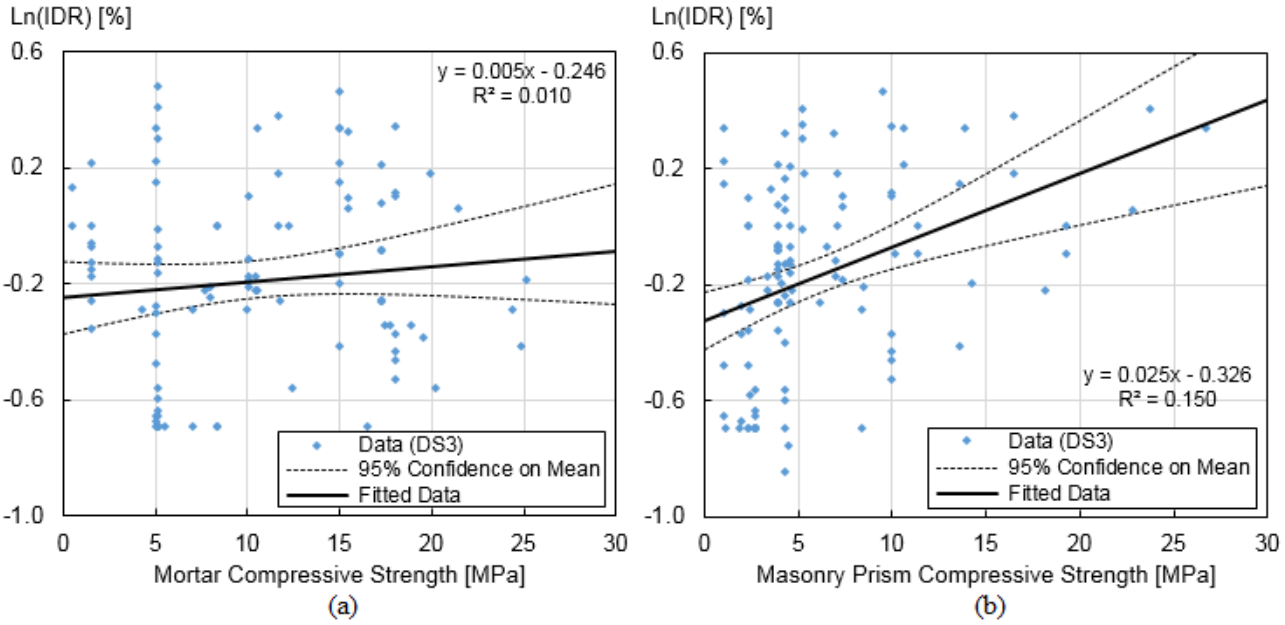

Fig. 12 Influence of mortar compressive strength (a) and prism compressive strength (b) on interstory drift ratios producing damage state DS_3.

As previously discussed, the influence of mortar compressive strength diminishes with increasing level of damage as illustrated by a decreasing slope in these figures. For this reason, we propose that the influence of mortar strength be considered only for damage state DS_1. Even though the coefficients of determination shown in Fig. 11(b) and Fig. 12(b) are relatively low, confidence intervals on the linear regression indicate that the positive slope, corresponding to a tendency to increase Ln(IDR) with increasing prism compressive strength, is statistically significant corroborating results of Table 9.

In particular, linear regressions represented in Fig. 10, Fig. 11 and Fig. 12 can be employed to compute the logarithmic mean $\mu_{\ln(\delta)}$ of the lognormal fit for the given damage state as a function of the mortar compressive strength as follows:

$$\mu_{\ln(\delta)}^{DS_1}(f_m) = a_\mu \cdot f_m + b_\mu \tag{11}$$

Analogously, it is now necessary to determine a continuous dependence of the logarithmic dispersion β on the mortar compressive strength. The variation of the dispersion of *IDR*s at which the given damage state is attained as a function of the mortar compressive strength is computed herein by using a moving window analysis in the compressive strength domain, with a 4 MPa wide window moving at increments of 2 MPa. Fig. 13(a) depicts the obtained variation of the logarithmic dispersion of the *IDR* with changes in mortar compressive strength for damage state DS_1. This variation of dispersion can be approximated by a linear regression, reported in Fig. 13(a) as well, together with the respective coefficients a_β, b_β, and R^2:

$$\beta^{DS_1}(f_m) = a_\beta \cdot f_m + b_\beta \tag{12}$$

As shown by a relatively high coefficient of determination R^2, this approximation captures reasonably well the variation of the dispersion parameter as a function of mortar compressive strength.

Fig. 13(b) shows the fragility surface resulting from the use of Eqs. (4), (11) and (12) for damage state DS_1. This surface provides a much better estimation of the probability of experiencing or exceeding damage state DS_1 when compared to the fragility function portrayed in Fig. 5(a) in which DS_1 is estimated only as a function of *IDR*. In a similar fashion, it is possible to build the fragility surface for damage state DS_3 by introducing the dependence on masonry prism compressive strength.

Fig. 14(a) depicts the computed change in logarithmic dispersion due to prism compressive strength from moving window analysis, whereas Fig. 14(b) portrays the corresponding fragility surface for damage state DS_3 resulting from the use of Eq. (4) and two additional equations analogous to (11) and (12) for masonry prism compressive strength. Again, by including information of the masonry prism compressive strength an improved estimate of the probability of reaching or exceeding the various damage states is achieved.

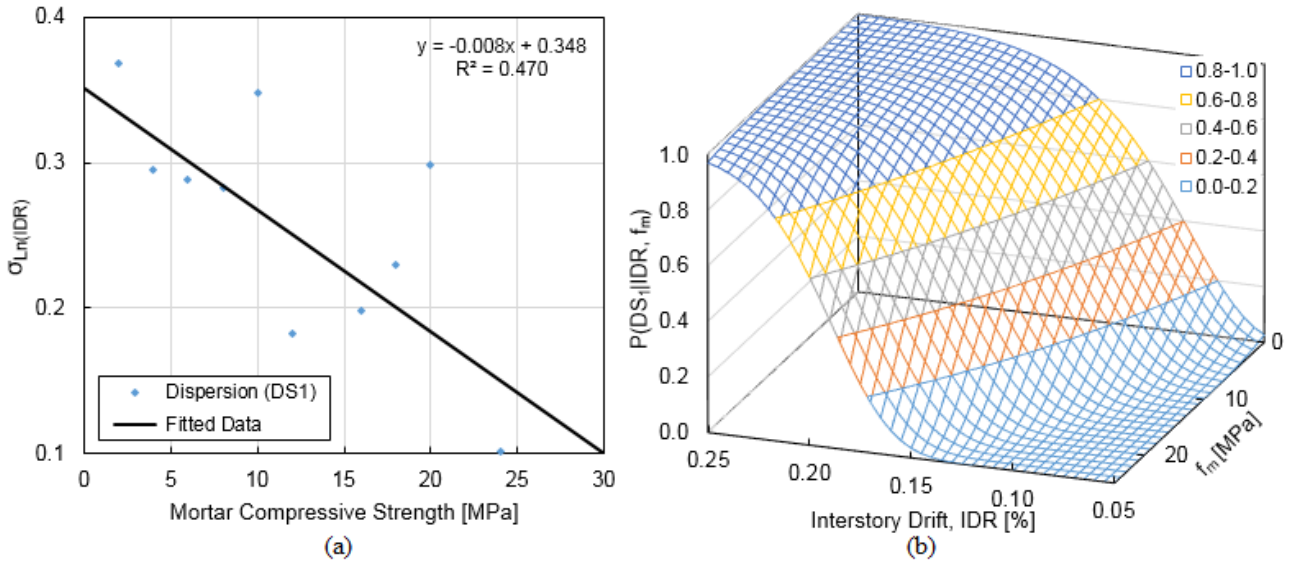

Fig. 13 (a) Variation of the logarithmic dispersion of the interstory drift ratio with changes in mortar compressive strength for damage state DS_1. (b) Proposed fragility surface to estimate damage state DS_1 as a function of *IDR* and compressive mortar strength.

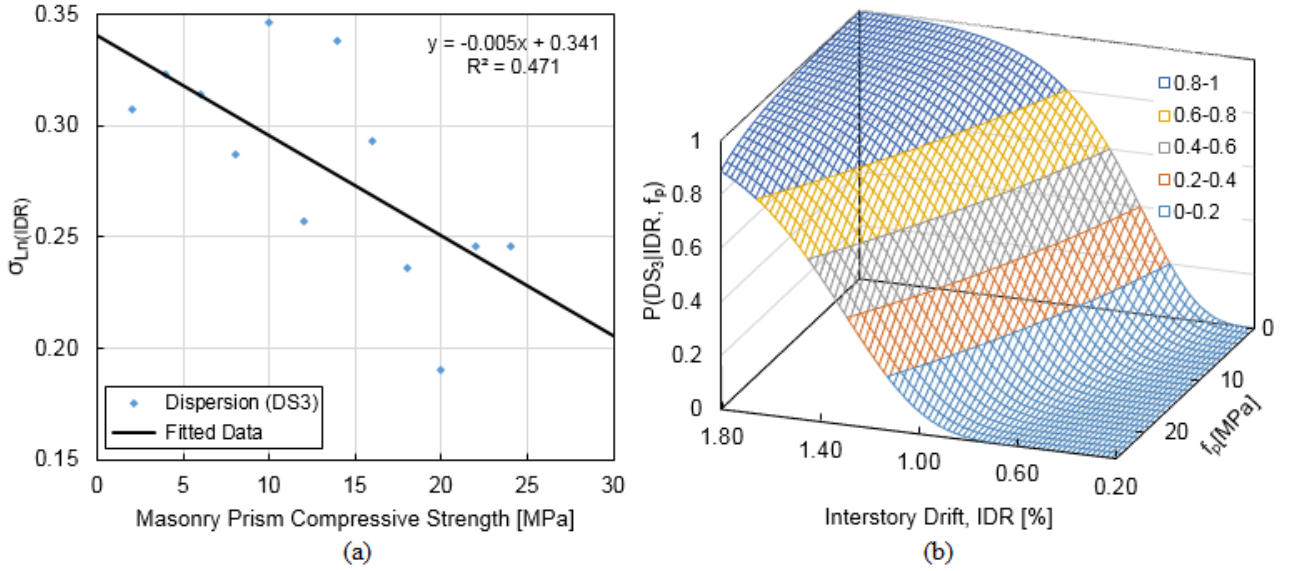

Fig. 14 (a) Variation of the logarithmic dispersion of the interstory drift ratio with changes in masonry prism compressive strength for damage state DS_3. (b) Proposed fragility surface to estimate damage state DS_3 as a function of both IDR and masonry prism compressive strength.

	DS_1: Light Cracking			DS_2: Moderate Cracking			DS_3: Heavy Cracking		
Openings	$\mu_{\ln(\delta)}$	β	# Spec.	$\mu_{\ln(\delta)}$	β	# Spec.	$\mu_{\ln(\delta)}$	β	# Spec.
W/ Openings	-2.350	0.109	22	-1.220	0.263	35	-0.227	0.341	38
W/O Openings	-1.993	0.330	79	-1.073	0.292	52	-0.175	0.330	95

Table 10. Statistical parameters estimated for interstory drift ratios corresponding to the three damage states in masonry infills with and without the presence of openings.

	DS_1: Light Cracking		DS_2: Moderate Cracking		DS_3: Heavy Cracking	
t-Test (openings)	$\Delta\mu$	$P(\lvert t\rvert > t^*_{5\%})$	$\Delta\mu$	$P(\lvert t\rvert > t^*_{5\%})$	$\Delta\mu$	$P(\lvert t\rvert > t^*_{5\%})$
W/ vs W/O	0.357	< **0.001**	0.147	**0.032**	0.052	**0.415**

Table 11. Results of the 5% significance level two-tailed *t*-tests on the difference between two logarithmic means for infills with and without openings. Shaded cell indicate that the null hypothesis cannot be rejected (i.e. no significant difference between means) for damage state DS_3.

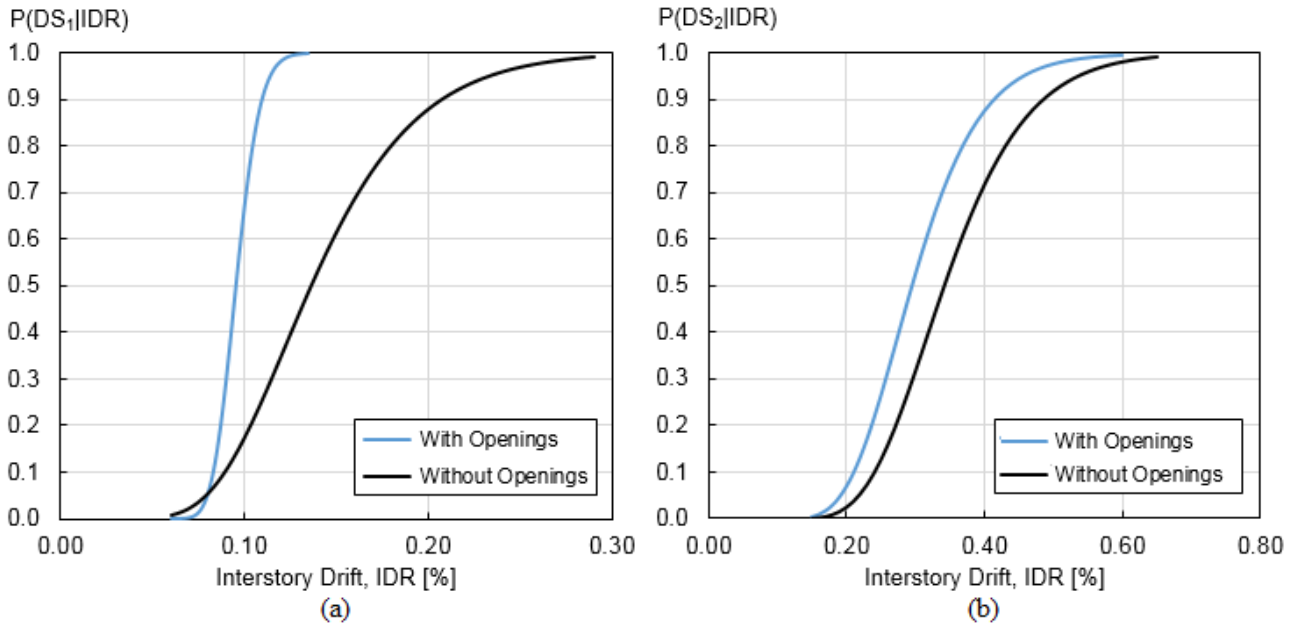

Fig. 15 Effect of opening on fragility functions for masonry infills for damage states DS_1 (a) and DS_2 (b).

4.4 Influence of openings

The presence of openings can also influence the *IDR* level at which infills experience a given damage state. Unfortunately, the number of specimens with openings in the initial dataset (38 specimens) is rather limited compared to the number of specimens without openings (114 specimens), thus preventing a combined analysis of the influence of openings and material compressive strength. However, it is still possible to assess whether the presence of openings in the specimens is significant by comparing *IDR* values at the onset of a given damage state in specimens with openings with *IDR* values at the onset of a given damage state for specimens without openings.

The procedure is based on two-tailed *t*-tests at a 5% significance level, and is analogous to that described in previous Subsections. The initial dataset has been subdivided into two subgroups: infills with openings and infills without openings. Fragility functions were computed by fitting a lognormal distribution to each dataset and for each damage state.

Table 10 contains statistical parameters for the lognormal distribution corresponding to fragility functions for the two subgroups of specimens for each of the three damage states. A summary of the tests of statistical significance is reported in Table 11. From an analysis of the results, it can be seen that the probability of reaching or exceeding damage states DS_1 and DS_2 is statistically different for infill masonry walls with and without openings respectively. However, no statistically significant influence was found for damage state DS_3.

From an analysis of the data, an *IDR* of 0.09% has a 50% probability of producing damage state DS_1 in infills with openings whereas an *IDR* of 0.125% is required for a 50% probability of infills without opening to be in DS_1. Fig. 15 portrays fragility curves of infills with and without openings for both damage states DS_1 and DS_2. It can be noted that, for damage state DS_1 the dispersion for infills with openings is much lower than the dispersion for infills without openings. Nevertheless, as stated previously, it should be pointed out that a relatively limited number of specimens with openings compared to the number of specimens without openings is available.

Moreover, it should benoted that, for damage state DS_2 the difference in dispersion between the two samples is smaller. If a bigger dataset was available for infills with openings, more complete evaluations could be made regarding the dimensions of openings and their position on the panel. Unfortunately, such information is not available at present time.

5. SUMMARY AND CONCLUSIONS

Drift-based fragility functions providing a probabilistic estimation of the level of damage experienced in masonry infill walls in reinforced concrete and steel frame buildings have been developed, for three damage states. The damage states have been defined based on damage patterns observed both in laboratory tests as well as those observed on damaged buildings after earthquakes and based on the associated repair actions. An extensive experimental dataset based on 33 investigations with a total of 152 specimens was assembled and used for the development of lognormal fragility curves and for the evaluation of the influence of different sources of uncertainty. Experimental results are limited to in-plane loading, thus the results are aimed at estimating only in-plane damage. Out-of-plane response or interaction of in-plane and out-of-plane loading are not accounted for. The hypothesis that lognormal distribution suitably describes collected data has been positively tested through a Lilliefors goodness-of-fit test. Moreover, fragility functions developed in this study have been accompanied by confidence bands accounting for finite-sample uncertainty.

From the analysis of various parameters that produce variability and therefore that introduce uncertainty in determining the damage state for a given masonry infill, it has been found that brick type does not seem to introduce a clear statistically significant influence on fragility functions, since in five out of nine null hypothesis tests at 5% significance could not be rejected. On the contrary, compressive strength of mortar is shown to significantly influence the attainment of lower damage states DS_1 and DS_2, whereas masonry prism compressive strength has a significant influence on all three damage states. For this reasons, bivariate fragility functions (fragility surfaces) have been developed taking into account both *IDR* and materials compressive strength for cases in which such information is available or can be estimated. Even if the sample size of specimens with openings was not large enough to allow an analysis of the influence of opening combined with other sources of variability, it has been shown that presence of openings significantly decreases the average *IDR* required to reach damage states DS_1 and DS_2, whereas no clear influence of openings was observed for damage state DS_3. However, this lack of statistical difference for DS_3 might be related to the fact that there was no out-of-plane loading applied to the specimens.

Finally, a comment on the influence of the infill wall/frame strength ratio should be made. The infill wall/frame strength ratio plays an important role in the combined hysteretic behavior of a frame/infill specimen, but much less in the damage to the infill wall. The latter is primarily the result of deformations in the infill, which are strongly correlated to the lateral deformations imposed on the frame. Furthermore, the distribution of resistance between the frame and the infill is deformation dependent, in other words changes as the level of deformation increases. So there is no unique way of defining infill wall/frame strength ratio. In addition, none of the experimental studies considered reports failure in the frame before the infill reaches damage state DS_3, whereas only a limited number of studies reports damage progression in the frame after failure of the infill.

The drift-based fragility functions developed in this study provide a tool for estimating damage in masonry infills and can be used in a probabilistic performance-based assessment framework. For cases in which no information of the mortar strength and/or prism masonry strength is available, fragility functions that are only a function of IDR can be used, whereas in cases in which the mortar strength and/or prism masonry strength are known or can be estimated, fragility surfaces are proposed, which provide an improved estimate of the probability of reaching or exceeding a given damage state.

6. ACKNOWLEDGEMENTS

Andrea Chiozzi would like to express his gratitude to Prof. Antonio Tralli and the "Young Researchers Fellowship" (5x1000 Funds, 2014) issued by the University of Ferrara, as well as the Civil Protection Department of Emilia-Romagna for the financial support provided to conduct the research reported in this paper. The authors are also grateful to Prof. Greg Deierlein, director of the John A. Blume Center for Earthquake Engineering at Stanford University, for comments and suggestions on this work. The authors would also like to thank the two anonymous reviewers for their comments and suggestions to improve our paper.

REFERENCES

1. Braga F, Manfredi V, Masi A, Salvatori A, Vona M. Performance of non-structural elements in RC buildings during the L'Aquila, 2009 earthquake. *Bulletin of Earthquake Engineering* 2011; **9**(1): 307–324. DOI: 10.1007/s10518-010-9205-7.

2. Miranda E, Mosqueda G, Retamales R, Pekcan G. Performance of Nonstructural Components during the 27 February 2010 Chile Earthquake. *Earthquake Spectra* 2012; **28**(S1): S453–S471. DOI: 10.1193/1.4000032.

3. Fierro EA, Miranda E, Perry CL. Behavior of Nonstructural Components in Recent Earthquakes. *AEI 2011*, Reston, VA: American Society of Civil Engineers; 2011. DOI: 10.1061/41168(399)44.

4. Toulkeridis T, Chunga K, Renterìa W, Rodriguez F, Mato F, Nikolaou S, *et al*. Mw 7.8 Muisne, Ecuador 4/16/16 Earthquake Observations: Geophysical Clustering, Intensity Mapping, Tsunami. *Proceedings of the 16th World Conference on Earthquake Engineering*, Santiago Chile: 2017.

5. Taghavi S, Miranda E. *Response assessment of nonstructural building elements*. Report No 2003/05, Pacific Earthquake Engineering Research Center, Berkeley: 2003.

6. Chiozzi A, Milani G, Grillanda N, Tralli A. A fast and general upper-bound limit analysis approach for out-of-plane loaded masonry walls. *Meccanica* 2017: in press. DOI: 10.1007/s11012-017-0637-x.

7. Colangelo F. Drift-sensitive non-structural damage to masonry-infilled reinforced concrete frames designed to Eurocode 8. *Bulletin of Earthquake Engineering* 2013; **11**(6): 2151–2176. DOI: 10.1007/s10518-013-9503-y.

8. Ricci P, De Risi MT, Verderame GM, Manfredi G. Influence of Infill Presence and Design Typology on Seismic Performance of RC Buildings: Fragility Analysis and Evaluation of Code Provisions at Damage Limitation Limit State. *Proceedings of the 15th World Conference on Earthquake Engineering*, Lisboa, Portugal: 2012.

9. Deierlein GG. *Overview of a comprehensive framework for performance earthquake assessment*. Report No 2004/05, Pacific Earthquake Engineering Research Center, Berkeley: 2004.

10. Krawinkler H, Miranda E. Performance-Based Earthquake Engineering. In: Bozorgnia Y, Bertero V, editors. *From Engineering Seismology to Performance-Based Engineering*, CRC Press; 2004.

11. Aslani H, Miranda E. *Probabilistic response assessment for building-specific loss estimation*. Report No 2003/03, Pacific Earthquake Engineering Research Center, Berekely: 2003.

12. Aslani H, Miranda E. Fragility Assessment of Slab-Column Connections in Existing Non-Ductile Reinforced Concrete Structures. *Journal of Earthquake Engineering* 2005; **9**(6): 777. DOI: 10.1142/S1363246905002262.

13. Ruiz-García J, Negrete M. Drift-based fragility assessment of confined masonry walls in seismic zones. *Engineering Structures* 2009; **31**(1): 170–181. DOI: 10.1016/j.engstruct.2008.08.010.

14. Cardone D, Perrone G. Developing fragility curves and loss functions for masonry infill walls. *Earthquake and Structures* 2015; **9**(1). DOI: http://dx.doi.org/10.12989/eas.2015.9.1.000.

15. Sassun K, Sullivan TJ, Morandi P, Cardone D. Characterising The In-Plane Seismic Performance of Infill Masonry. *Bulletin of the New Zealand Society for Earthquake Engineering* 49AD; **1**.

16. Kadysiewski S, Mosalam KM. *Modeling of Unreinforced Masonry Infill Walls Considering In-Plane and Out-of-Plane Interaction*. Berkeley: 2008.

17. Di Trapani F, Macaluso G, Cavaleri L, Papia M. Masonry infills and RC frames interaction: literature overview and state of the art of macromodeling approach. *European Journal of Environmental and Civil Engineering* 2015; **19**(9): 1059–1095. DOI: 10.1080/19648189.2014.996671.

18. Mehrabi AB, Benson Shing P, Schuller MP, Noland JL. Experimental Evaluation of Masonry-Infilled RC Frames. *Journal of Structural Engineering* 1996; **122**(3): 228–237. DOI: 10.1061/(ASCE)0733-9445(1996)122:3(228).

19. Kakaletsis DJ, Karayannis CG. Experimental Investigation of Infilled Reinforced Concrete Frames with Openings. *ACI Structural Journal* 2009; **106**(2). DOI: 10.14359/56351.

20. Dawe JL, Yong TD. An Investigation of Factors Influencing the Behaviour of Masonry Infill in Steel Frames Subjected to In-Plane Shear. *Proceedings of the 7th International Brick and Block Masonry Conference*, Melbourne, Australia: 1985.

21. Akhound F, Vasconcelos G, Lourenço PB, Palha CAOF, Silva LC. In-plane and out-of plane experimental characterization of rc masonry infilled frames. *M2D - 6th International Conference on Mechanics and Materials in Design* 2015: 427–440.

22. Al-Chaar G, Issa M, Sweeney S. Behavior of Masonry-Infilled Nonductile Reinforced Concrete Frames. *Journal of Structural Engineering* 2002; **128**(8): 1055–1063. DOI: 10.1061/(ASCE)0733-9445(2002)128:8(1055).

23. Angel R, Abrams DP, Shapiro D, Uzarski J, Webster M. Behavior of Reinforced Concrete Frames with Masonry Infills 1994.

24. Basha SH, Kaushik HB. Behavior and failure mechanisms of masonry-infilled RC frames (in low-rise buildings) subject to lateral loading. *Engineering Structures* 2016; **111**: 233–245. DOI: 10.1016/j.engstruct.2015.12.034.

25. Bergami AV, Nuti C. Experimental tests and global modeling of masonry infilled frames. *Earthquakes and Structures* 2015; **9**(2): 281–303. DOI: 10.12989/eas.2015.9.2.281.

26. Calvi GM, Bolognini D, Penna A. Seismic Performance Of Masonry-Infilled RC Frames, Benefits Of Slight Reinforcements. *Proceedings of the 6th National Congress in Seismology and Earthquake Engineering*, Guimarães, Portugal: University of Minho; 2004.

27. Chiou TC, Hwang SJ. Tests on cyclic behavior of reinforced concrete frames with brick infill. *Earthquake Engineering & Structural Dynamics* 2015; **44**(12): 1939–1958. DOI: 10.1002/eqe.2564.

28. Colangelo F. Pseudo-dynamic seismic response of reinforced concrete frames infilled with non-structural brick masonry. *Earthquake Engineering & Structural Dynamics* 2005; **34**(10): 1219–1241. DOI: 10.1002/eqe.477.

29. Crisafulli FJ. Seismic behaviour of reinforced concrete structures with masonry infills. University of Canterbury, 1997.

30. Guidi G, da Porto F, Dalla Benetta M, Verlato N, Modena C. Comportamento Sperimentale nel Piano e Fuori Piano di Tamponamenti in Muratura Armata e Rinforzata. *Ingenio* 2013; **23**.

31. Flanagan RD, Bennett RM. In-Plane Behavior of Structural Clay Tile Infilled Frames. *http://dx.doi.org/101061/(ASCE)0733-9445(1999)125:6(590)* 1999. DOI: 10.1061/(ASCE)0733-9445(1999)125:6(590).

32. Gazić G, Sigmund V. Ciklična ispitivanja jednorasponskih slabih okvira sa zidanom ispunom. *Journal of the Croatian Association of Civil Engineers* 2016; **68**(8): 617–633. DOI: 10.14256/JCE.1614.2016.

33. Guerrero N, Martínez M, Picón R, Marante ME, Hild F, Roux S, *et al*. Experimental analysis of masonry infilled frames using digital image correlation. *Materials and Structures* 2014; **47**(5): 873–884. DOI: 10.1617/s11527-013-0099-0.

34. Haider S. In-Plane Cyclic Response of Reinforced Concrete Frames With Unreinforced Masonry Infills. Rice University, 1995.

35. Jiang H, Liu X, Mao J. Full-scale experimental study on masonry infilled RC moment-resisting frames under cyclic loads. *Engineering Structures* 2015; **91**: 70–84. DOI: 10.1016/j.engstruct.2015.02.008.

36. Khoshnoud HR, Marsono K. Experimental study of masonry infill reinforced concrete frames with and without corner openings. *Structural Engineering and Mechanics* 2016; **57**(4): 641–656. DOI: http://dx.doi.org/10.12989/sem.2016.57.4.641.

37. Liu Y, Soon S. Experimental study of concrete masonry infills bounded by steel frames. *Canadian Journal of Civil Engineering* 2012; **39**(2): 180–190. DOI: 10.1139/l11-122.

38. Mansouri A, Marefat MS, Khanmohammadi M. Experimental evaluation of seismic performance of low-shear strength masonry infills with openings in reinforced concrete frames with deficient seismic details. *The Structural Design of Tall and Special Buildings* 2014; **23**(15): 1190–1210. DOI: 10.1002/tal.1115.

39. Markulak D, Radić I, Sigmund V. Cyclic testing of single bay steel frames with various types of masonry infill. *Engineering Structures* 2013; **51**: 267–277. DOI: 10.1016/j.engstruct.2013.01.026.

40. Misir IS, Ozcelik O, Girgin SC, Yucel U. The Behavior of Infill Walls in RC Frames Under Combined Bidirectional Loading. *Journal of Earthquake Engineering* 2016; **20**(4): 559–586. DOI: 10.1080/13632469.2015.1104748.

41. Morandi P, Hak S, Magenes G. In-Plane Experimental Response of Strong Masonry Infills. *Proceedings of the 9th International Masonry Conference*, Guimarães, Portugal: International Masonry Society; 2014. DOI: 10.13140/2.1.4206.5280.

42. Mosalam KM, White RN, Gergely P. Static Response of Infilled Frames Using Quasi-Static Experimentation. *Journal of Structural Engineering* 1997; **123**(11): 1462–4169. DOI: 10.1061/(ASCE)0733-9445(1997)123:11(1462).

43. Preti M, Migliorati L, Giuriani E. Experimental testing of engineered masonry infill walls for post-earthquake

structural damage control. *Bulletin of Earthquake Engineering* 2015; **13**(7): 2029–2049. DOI: 10.1007/s10518-014-9701-2.

44. Pujol S, Benavant-Climent A, Rodriguez ME, Smith-Pardo J. Masonry Infill Walls: an Effective Alternative for Seismic Strengthening of Low-Rise Reinforced Concrete Building Structures. *Proceedings of the 14th World Conference on Earthquake Engineering*, Beijing, China: 2008.

45. Sanchez Tizapa S. Experimental and numerical study of confined masonry walls under in-plane loads, case: Guerrero State (Mexico). Université Paris-Est, 2010.

46. Schneider SP, Zagers BR, Abrams DP. Lateral Strength of Steel Frames with Masonry Infills Having Large Openings. *Journal of Structural Engineering* 1998; **124**(8): 896–904. DOI: 10.1061/(ASCE)0733-9445(1998)124:8(896).

47. Sigmund V, Penava D. Influence of Openings, With and Without Confinement, on Cyclic Response of Infilled R-C Frames — An Experimental Study. *Journal of Earthquake Engineering* 2014; **18**(1): 113–146. DOI: 10.1080/13632469.2013.817362.

48. Tasnimi AA, Mohebkhah A. Investigation on the behavior of brick-infilled steel frames with openings, experimental and analytical approaches. *Engineering Structures* 2011; **33**(3): 968–980. DOI: 10.1016/j.engstruct.2010.12.018.

49. Zarnic R, Tomazevic M. The Behaviour of Masonry Infilled Reinforced Concrete Frames Subjected to Cyclic Lateral Loading. *Proceedings of the 9th World Conference on Earthquake Engineering*, Tokyo-Kyoto, Japan: 1988.

50. Zovkic J, Sigmund V, Guljas I. Cyclic testing of a single bay reinforced concrete frames with various types of masonry infill. *Earthquake Engineering & Structural Dynamics* 2013; **42**(8): 1131–1149. DOI: 10.1002/eqe.2263.

51. Blom G. *Statistical Estimates and Transformed Beta-Variables*. Wiley; 1958.

52. Cunnane C. Unbiased plotting positions — A review. *Journal of Hydrology* 1978; **37**(3): 205–222. DOI: 10.1016/0022-1694(78)90017-3.

53. Benjamin J, Cornell A, Shaw H. *Probability, statistics, and decisions for civil engineers*. Mcgraw-Hill; 1963.

54. Lilliefors HW. On the Kolmogorov-Smirnov Test for Normality with Mean and Variance Unknown. *Journal of the American Statistical Association* 1967; **62**(318): 399. DOI: 10.2307/2283970.

55. Crow EL, Davis FA, Maxfield MW. *Statistics Manual*. New York: Dover Publication; 1960.

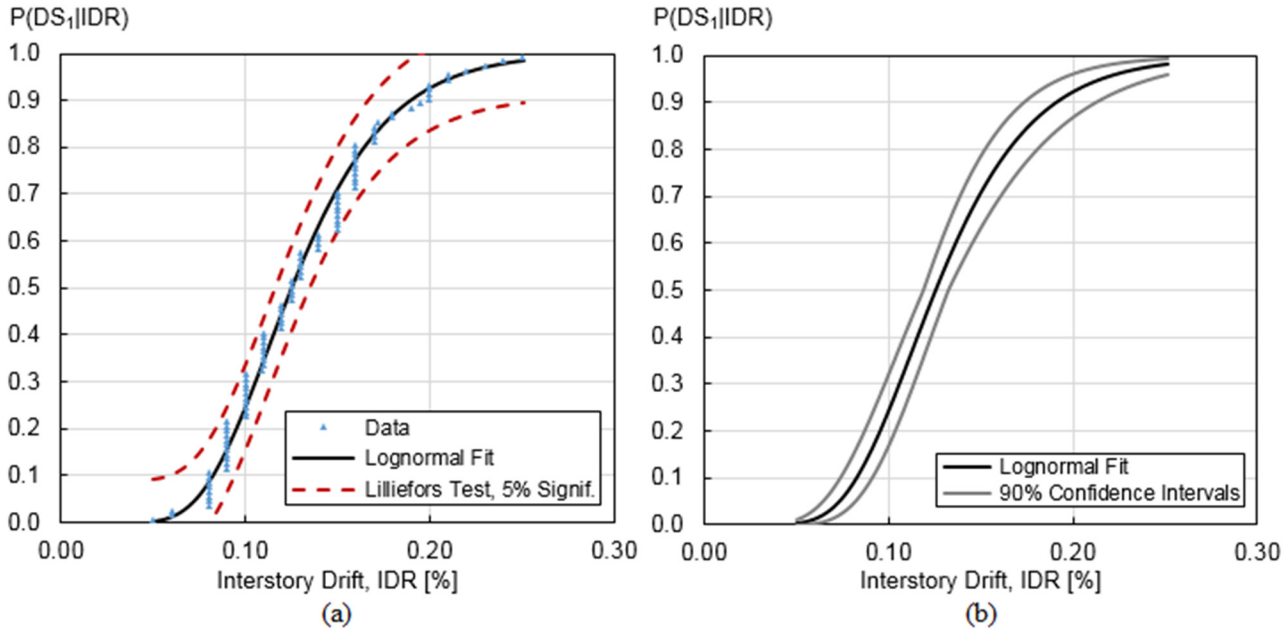

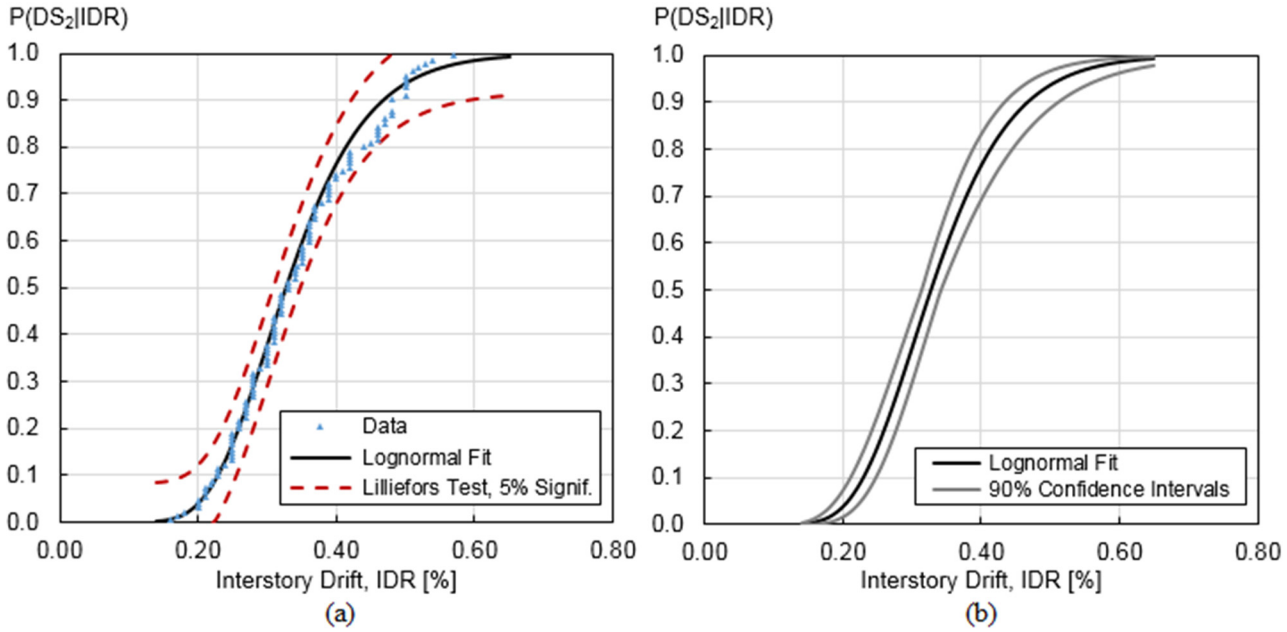

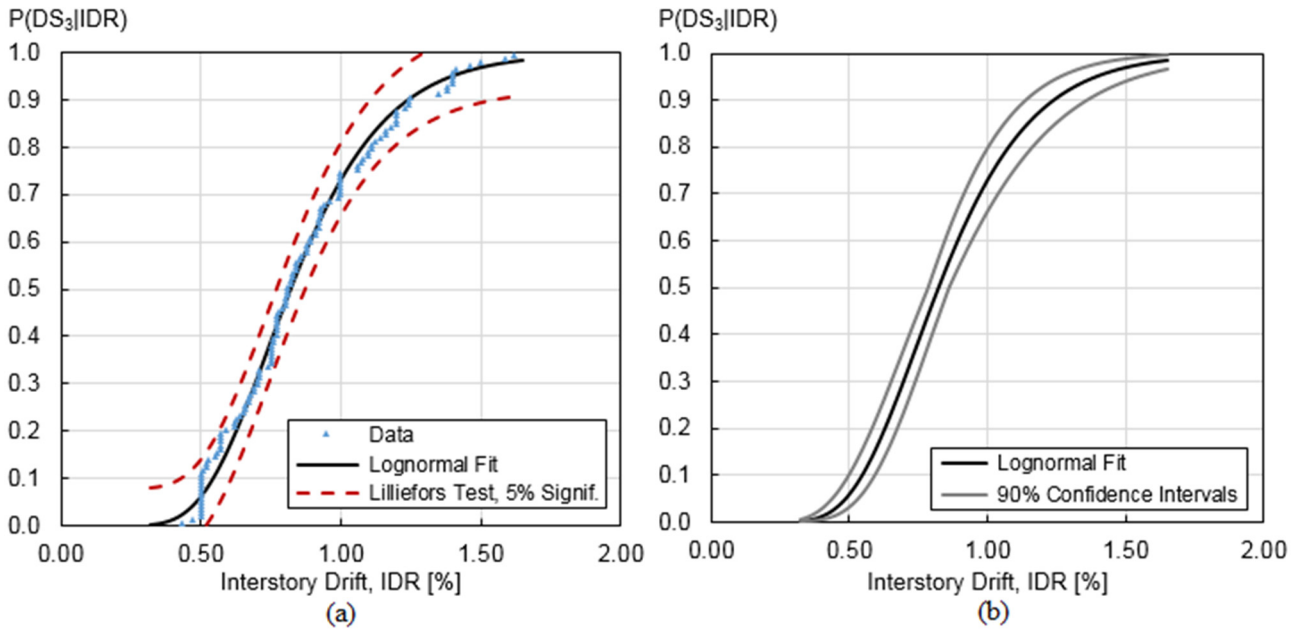

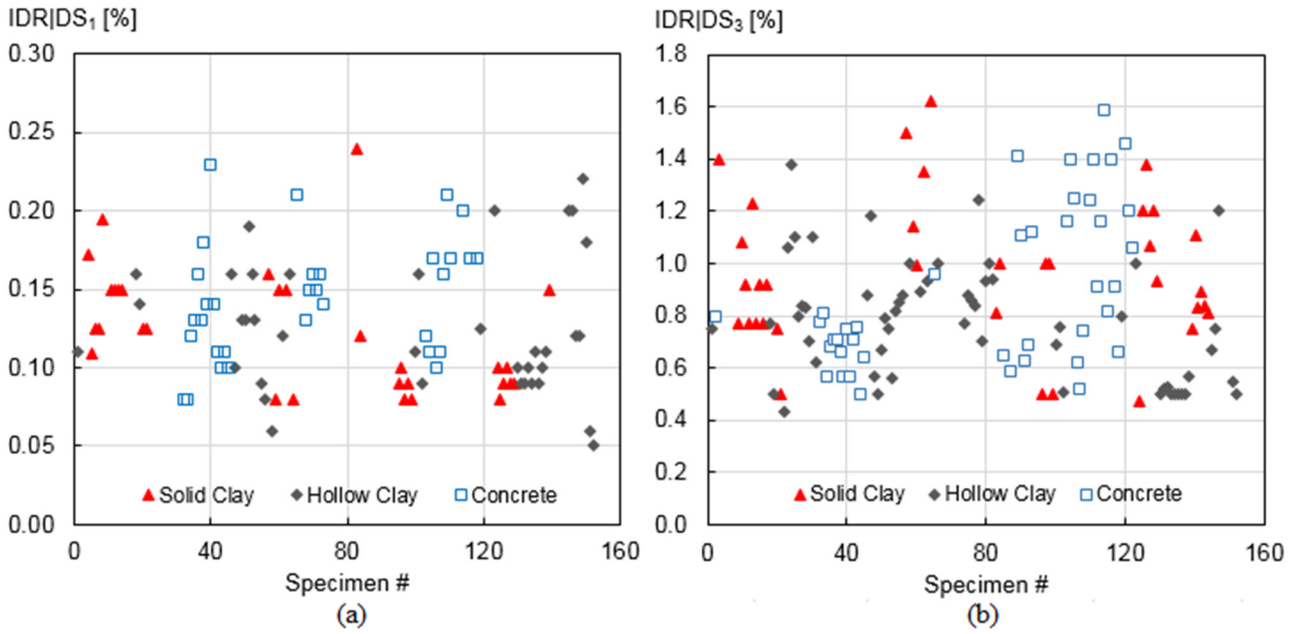

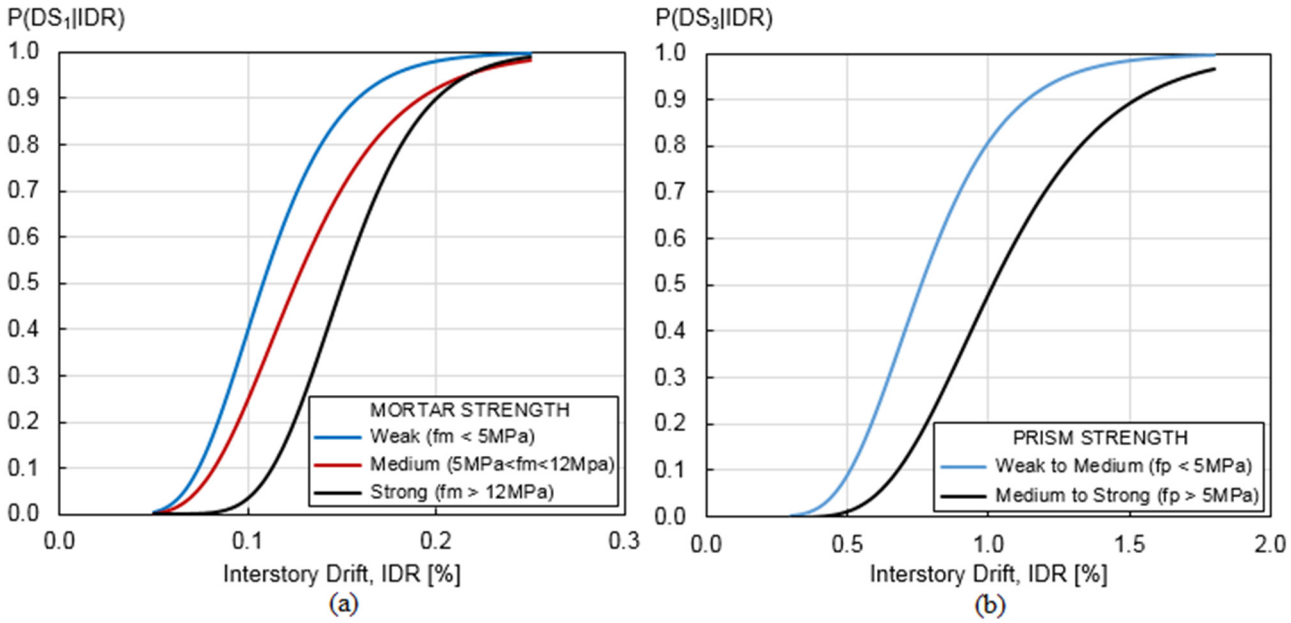

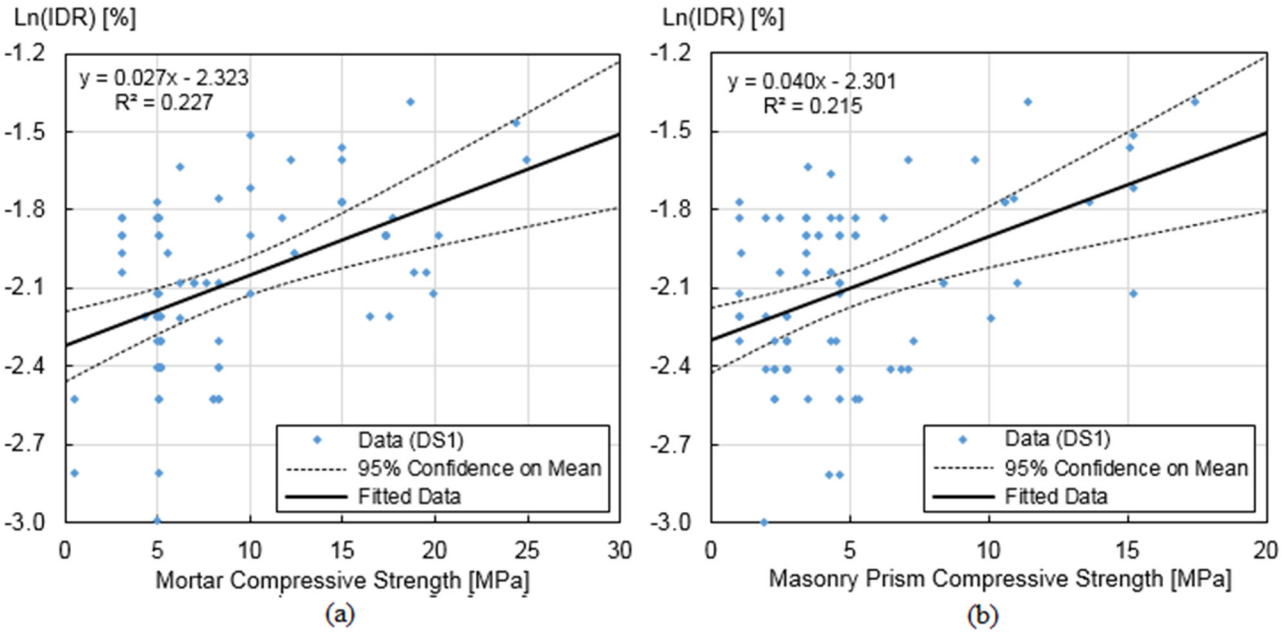

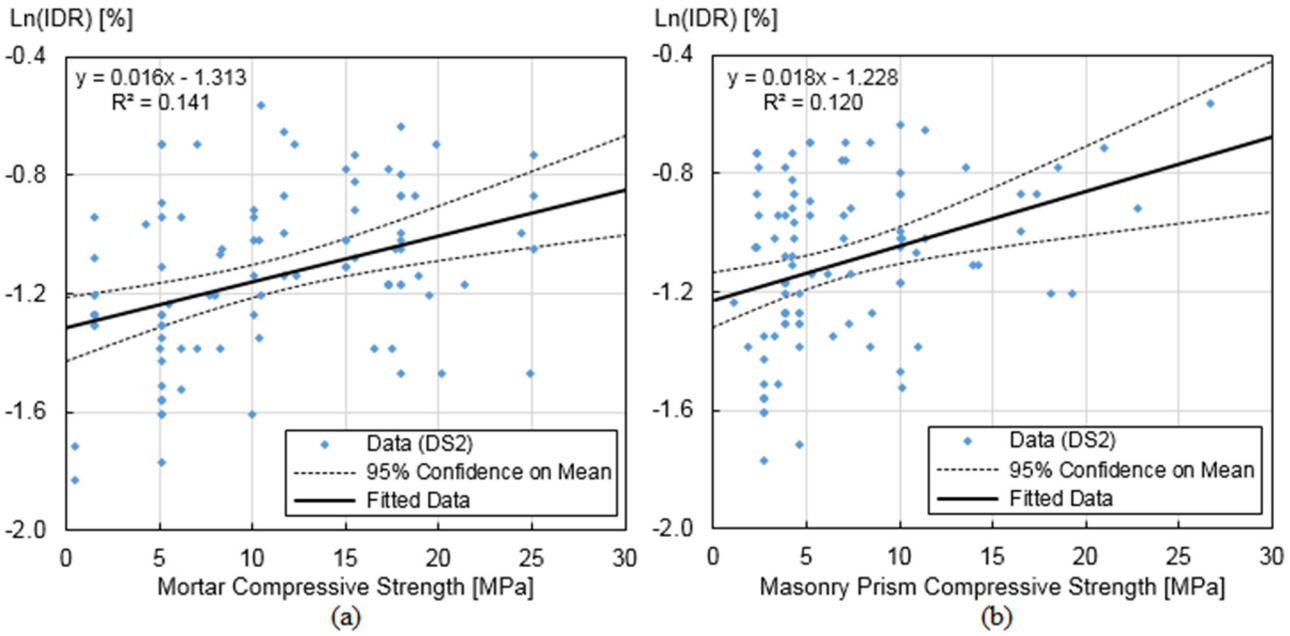

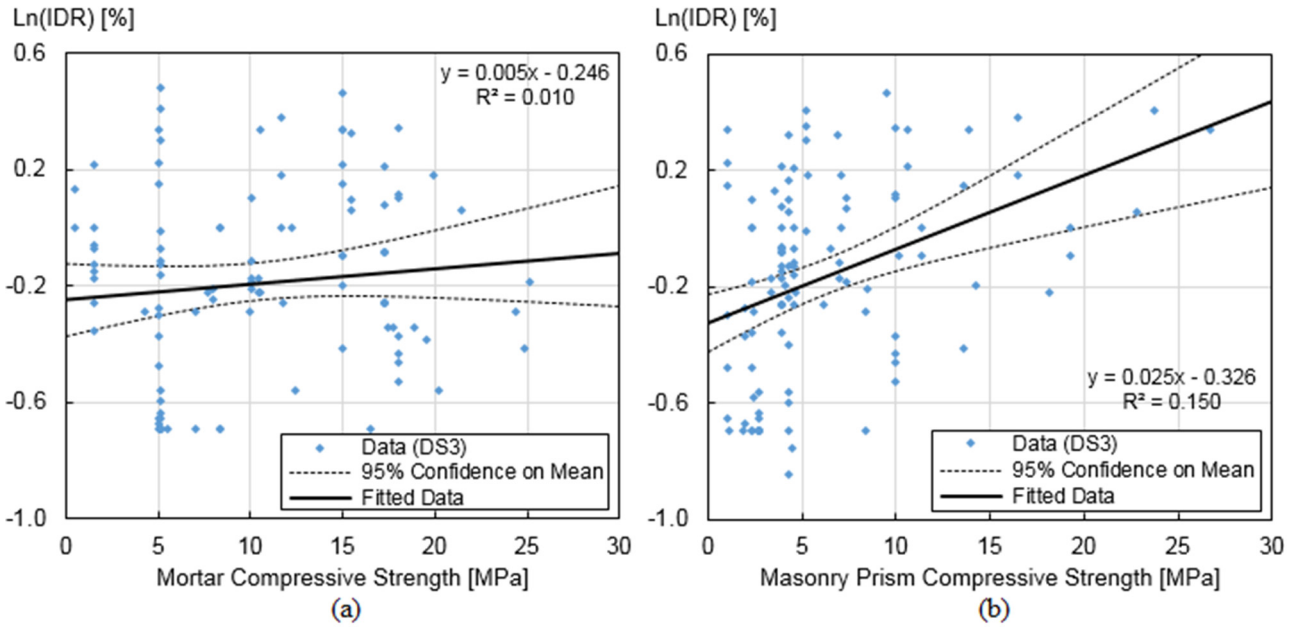

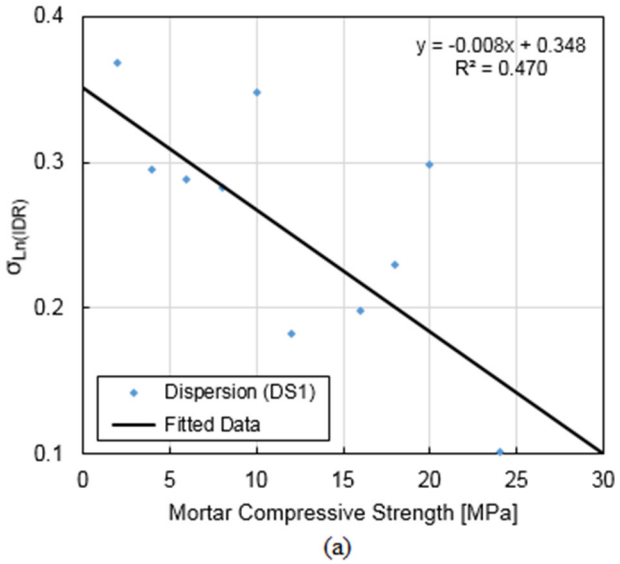

(a)

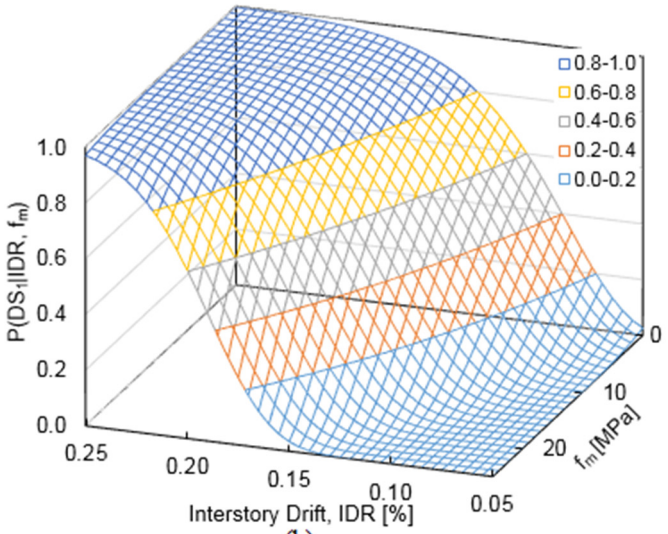

(b)

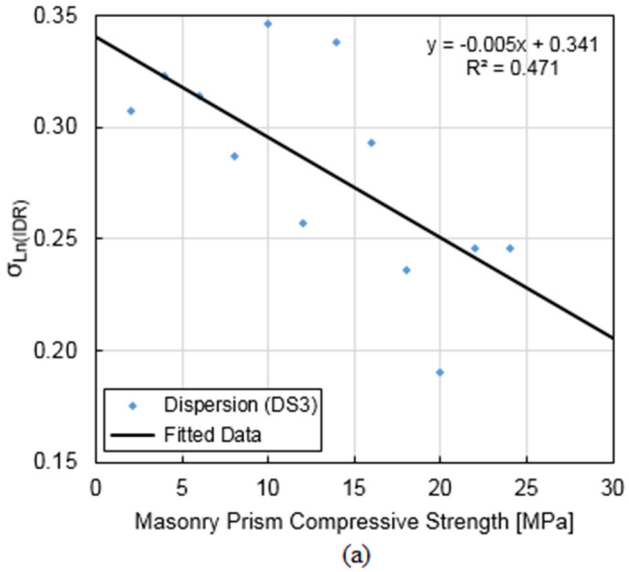

(a)

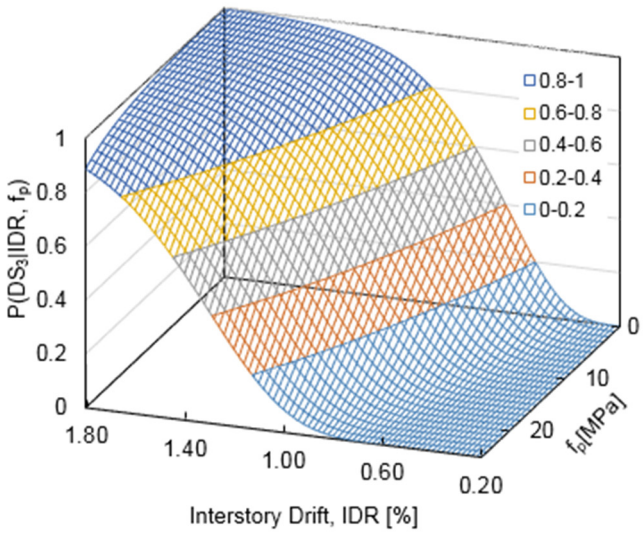

(b)

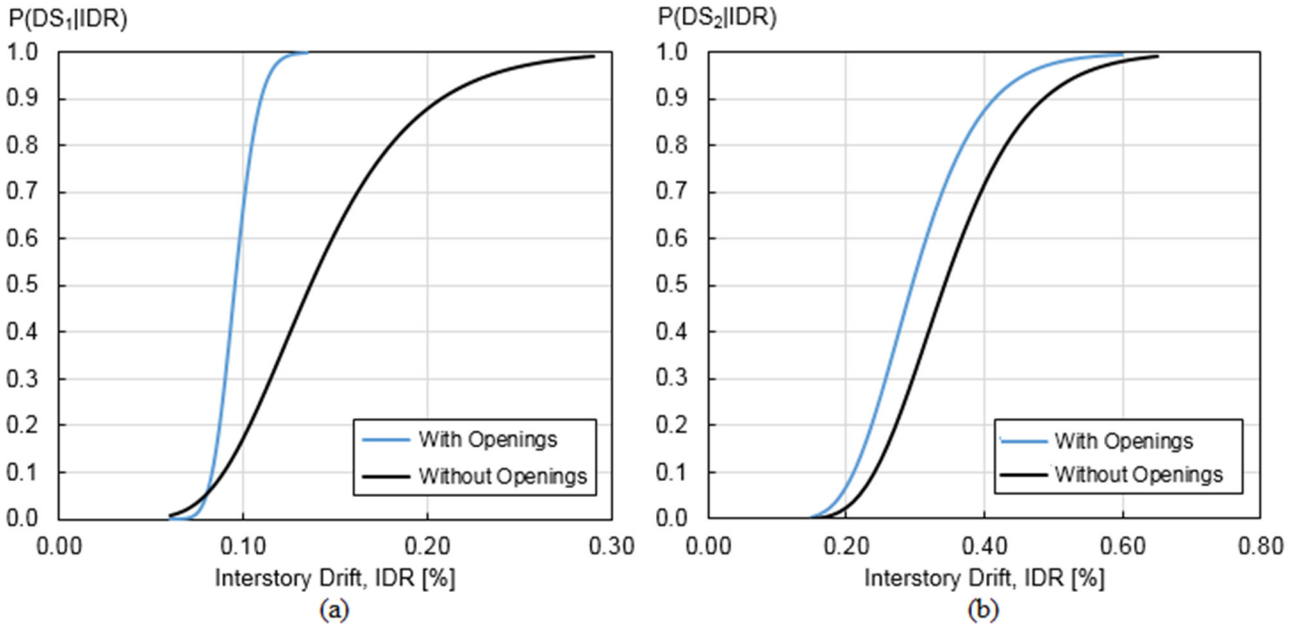

Ref.	# Spec.	Scale	Masonry Unit	Mortar CS f_m [MPa]	Prism CS f_p [MPa]	Thickness t [m]	Length L [m]	Height H [m]	Openings
[19]	1	1:2 RC	HCB	4.3	n.d.	0.080	2.415	1.635	w/o
[20]	2	1:2 RC	CMU(1)-SCB(1)	10.5	18.1-26.7	0.06-0.1	1.829	1.327	w/o
[21]	5	1:1 RC	SCB	6.2-8.3	3.5-11.0	0.047-0.187	2.438	1.626	w/o
[22]	9	1:2 RC	SFB	17.3	3.9-4.6	0.055-0.110	1.500	1.500	w/o
[23]	1	1:2 RC	HCB	11.7	V=6.2; H=2.9	0.120	2.300	1.300	w/o
[24]	1	1:1 RC	HCB	5.5	1.1	0.115	4.200	2.750	w/o
[25]	2	1:1 RC	SCB	7.0	8.4	0.200	3.2-6.8	2.640	w/o
[26]	10	1:2 RC	HCB	10.4-25.1	V=2.2-5.1; H=2.5-3.9	0.120-0.160	1.7-2.3	1.300	w/o
[27]	2	3:4 RC	SCrB	8.0	19.3	0.090	2.516	2.000	w/o
[28]	1	1:1 RC	HCB	19.9	n.d.	0.300	4.450	2.680	w/o
[18]	12	1:1 RC	CMU	12.4-24.4	17.4-35.4	0.200	3.600	2.800	w/o
[29]	9	1:1 S	HCB	medium	V=2.3-5.6; H=2.6-4.1	0.195-0.330	2.2-7.3	2.2-6.2	w/o
[30]	10	1:2 RC	HCB(4)-SCB(6)	0.5-5.1	3.5-5.2	0.12	1.85	1.3	w/o
[31]	1	n.d.	CMU	n.d.	n.d.	0.150	2.400	1.550	w/o
[32]	2	1:1 RC	HCB	11.7-18.7	11.4-17.4	0.089	2.007	2.070	w/o
[33]	6	1:1 RC	ACB	3.1	3.5	0.200	5.240	2.725	w/o
[17]	9	1:3 RC	HCB	1.5	V=2.6 H=5.1	0.093	1.200	0.800	w/o(1) -w(8)
[34]	2	1:4 RC	SCB	n.d.	n.d.	0.060	0.900	0.700	w/o(1)-w(1)
[35]	10	1:3 S	CMU	18.0	10.0	0.067	1.1-1.7	1.080	w/o(8)-w(2)
[36]	5	1:2 RC	SCB	8.3	2.3	0.106	2.100	1.300	w/o(1) -w(4)
[37]	9	1:2 S	HCB(3)-ACB(6)	5.0	1.0-2.0	0.125-0.190	2.062	1.556	w/o
[16]	10	1:2 RC	CMU(4)-SCrB(6)	15.0	9.5-15.1	0.092	2.057	1.422	w/o
[38]	2	1:2 RC	HCB	medium	n.d.	0.120	2.000	1.250	w/o
[39]	1	1:1 RC	HCB	7.7	4.6	0.350	4.220	2.950	w/o
[40]	3	1:4 S	HCB	11.7-21.4	16.5-22.8	0.100	1.800	0.940	w/o(1)-w(2)
[41]	1	1:1 S	HCB	12.2	7.1	0.190	2.930	2.460	w/o
[42]	1	1:1 RC	SCB	10.0	n.d.	0.092	6.100	3.050	w/o
[43]	1	1:2 S	SCB	28.0	4.5	0.130	2.100	1.650	w/o
[44]	5	1:1 S	SCB	low	5.3-7.3	0.1-0.2	2.740	1.676	w
[45]	9	1:2 RC	HCB	5.2	2.7	0.120	2.000	1.400	w/o(1)-w(8)
[46]	5	1:1 S	SCB	10.1	7.0-8.5	0.110	2.260	1.800	w/o(1)-w(4)
[47]	3	1:2 RC	HCB	10.0	15.2	0.120	2.080	1.500	w/o
[48]	2	1:2 RC	HCB	5.0-5.1	1.9-4.3	0.120	1.800	1.300	w/o

SCB: Solid Clay Bricks; HCB: Hollow Clay Bricks; CMU: Concrete Masonry Units; SCrB: Solid Concrete Blocks; ACB: AAC Blocks
RC: Reinforced Concrete; S: Steel; CS: Compressive Strength; V: Vertical compressive strength; H: Horizontal compressive strength.

Damage State	$\overline{IDR}$ [%]	$\mu_{\ln(\delta)}$	β	Number of Specimens
DS_1: light cracking	0.125	-2.078	0.325	100
DS_2: moderate cracking	0.327	-1.118	0.278	118
DS_3: heavy cracking	0.820	-0.198	0.320	132

Damage State	$\overline{IDR}$ *range* [%]	$\mu_{\ln(\delta)}$	β
DS_1: light cracking	0.119 ÷ 0.132	-2.078 ± 0.054	0.325 ± 0.043
DS_2: moderate cracking	0.314 ÷ 0.341	-1.118 ± 0.042	0.278 ± 0.034
DS_3: heavy cracking	0.784 ÷ 0.859	-0.198 ± 0.046	0.320 ± 0.037

	DS_1: Light Cracking			DS_2: Moderate Cracking			DS_3: Heavy Cracking		
Brick Type	$\mu_{\ln(\delta)}$	β	# Spec.	$\mu_{\ln(\delta)}$	β	# Spec.	$\mu_{\ln(\delta)}$	β	# Spec.
Solid Clay	-2.139	0.300	30	-1.087	0.299	31	-0.127	0.262	35
Hollow Clay	-2.136	0.355	37	-1.146	0.301	50	-0.298	0.293	56
Concrete Unit	-1.974	0.270	40	-1.104	0.221	34	-0.160	0.331	41

	DS_1: Light Cracking		DS_2: Moderate Cracking		DS_3: Heavy Cracking	
t-Test (brick type)	$\Delta\mu$	$P(\lvert t\rvert > t^*_{5\%})$	$\Delta\mu$	$P(\lvert t\rvert > t^*_{5\%})$	$\Delta\mu$	$P(\lvert t\rvert > t^*_{5\%})$
SC vs HC	0.003	**0.975**	0.058	**0.397**	0.171	**0.006**
SC vs CR	0.165	**0.027**	0.017	**0.795**	0.033	**0.631**
HC vs CR	0.162	**0.039**	0.041	**0.496**	0.137	**0.030**

	DS_1: Light Cracking			DS_2: Moderate Cracking			DS_3: Heavy Cracking		
Mortar Strength	$\mu_{\ln(\delta)}$	β	# Spec.	$\mu_{\ln(\delta)}$	β	# Spec.	$\mu_{\ln(\delta)}$	β	# Spec.
Weak	-2.226	0.298	43	-1.266	0.293	37	-0.213	0.365	46
Medium	-2.077	0.333	35	-1.062	0.259	37	-0.175	0.287	39
Strong	-1.894	0.224	23	-1.036	0.223	42	-0.145	0.352	48

	DS_1: Light Cracking		DS_2: Moderate Cracking		DS_3: Heavy Cracking	
t-Test (mortar)	$\Delta\mu$	$P(\lvert t\rvert > t^*_{5\%})$	$\Delta\mu$	$P(\lvert t\rvert > t^*_{5\%})$	$\Delta\mu$	$P(\lvert t\rvert > t^*_{5\%})$
W vs S	0.332	**0.001**	0.229	**0.001**	0.171	**0.361**
W vs M	0.149	**0.041**	0.204	**0.002**	0.033	**0.600**
M vs S	0.183	**0.015**	0.026	**0.642**	0.137	**0.663**

	DS_1: Light Cracking			DS_2: Moderate Cracking			DS_3: Heavy Cracking		
Prism Strength	$\mu_{\ln(\delta)}$	β	# Spec.	$\mu_{\ln(\delta)}$	β	# Spec.	$\mu_{\ln(\delta)}$	β	# Spec.
Weak to Medium	-2.163	0.301	54	-1.187	0.292	52	-0.273	0.312	71
Medium to Strong	-1.974	0.375	29	-1.008	0.238	45	0.016	0.317	44

	DS_1: Light Cracking		DS_2: Moderate Cracking		DS_3: Heavy Cracking	
t-Test (prism)	$\Delta\mu$	$P(\lvert t\rvert > t^*_{5\%})$	$\Delta\mu$	$P(\lvert t\rvert > t^*_{5\%})$	$\Delta\mu$	$P(\lvert t\rvert > t^*_{5\%})$
W vs S	0.190	**0.014**	0.178	**0.002**	0.289	**0.001**

	DS_1: Light Cracking			DS_2: Moderate Cracking			DS_3: Heavy Cracking		
Openings	$\mu_{\ln(\delta)}$	β	# Spec.	$\mu_{\ln(\delta)}$	β	# Spec.	$\mu_{\ln(\delta)}$	β	# Spec.
W/ Openings	-2.350	0.109	22	-1.220	0.263	35	-0.227	0.341	38
W/O Openings	-1.993	0.330	79	-1.073	0.292	52	-0.175	0.330	95

	DS_1: Light Cracking		DS_2: Moderate Cracking		DS_3: Heavy Cracking	
t-Test (openings)	$\Delta\mu$	$P(\lvert t\rvert > t^*_{5\%})$	$\Delta\mu$	$P(\lvert t\rvert > t^*_{5\%})$	$\Delta\mu$	$P(\lvert t\rvert > t^*_{5\%})$
W/ vs W/O	0.357	**< 0.001**	0.147	**0.032**	0.052	**0.415**